AUTHORIZATION TO LEND AND REPRODUCE THE THESIS

As the sole author of this thesis, I authorize Brown University to lend it to other institutions or individuals for the purpose of scholarly research.

Date_____ _____
Liana Kramer, Author

I further authorize Brown University to reproduce this thesis by photocopying or other means, in total or in part, at the request of other institutions or individuals for the purpose of scholarly research.

Date_____ _____
Liana Kramer, Author

Advancing an in vivo-relevant three-dimensional neural spheroid model for CNS disease modeling

by

Liana L. Kramer

Sc.B., Brown University, 2017

Submitted in partial fulfillment of the requirements for the degree of Master of Science in Biotechnology in the Division of Biology and Medicine at Brown University

Department of Molecular Pharmacology, Physiology, and Biotechnology

PROVIDENCE, RHODE ISLAND

MAY 2017

This thesis by Liana L. Kramer is accepted in its present form by the Division of Biology and Medicine as satisfying the thesis requirements for the degree of Master of Science.

Date_____ _____
Diane Hoffman-Kim, Ph.D., Advisor

Recommended to the Graduate Council

Date_____ _____
Jacquelyn Schell, Ph.D., Reader

Date_____ _____
Ulrike Mende, M.D., Reader

Approved by the Graduate Council

Date_____ _____
Peter Weber, Dean of the Graduate School

Curriculum Vitae

EDUCATION

Brown University, Providence, RI

Sc.M. Biotechnology
Advisor: Diane Hoffman-Kim, Ph.D.
Title of Thesis: Advancing an in-vivo relevant three-dimensional neural spheroid model for CNS disease modeling
Expected: May, 2017

Brown University, Providence, RI

Sc.B. Biology
Expected: May, 2017

PUBLICATIONS

Boutin, M., **Kramer, L.**, Livi, L., Brown, T., Moore C., & Hoffman-Kim, D. (2017). A Three-Dimensional Neural Spheroid Model for Capillary- Like Network Formation. *Journal of Neuroscience Methods.* DOI: 10.1016/j.jneumeth.2017.01.014

Alem, F., Yao, K., Lane, D., Calvert, V., Petricoin, E., **Kramer, L.**, Hale, M., Bavari, S., Panchal, R., & Hakami, R. (2015). Host response during Yersinia pestis infection of human bronchial epithelial cells involves negative regulation of autophagy and suggests a modulation of survival-related and cellular growth pathways. *Frontiers in Microbiology*. 6(50). DOI: 10.3389/fmicb.2015.00050

CONFERENCE ABSTRACTS

Boutin M., Sevetson, J., **Kramer, L.**, Hoffman-Kim, D. Understanding neurovascular endothelial cell migration using *in vitro* three dimensional models. Society for Neuroscience Annual Meeting, San Diego, CA, 2016.

AWARDS

2017 Fulbright U.S. Student Grantee

2017 Society of Sigma Xi Initiate

2016 Brown Graduate Student Conference Travel Award

2015, 2016 Karen T. Romer Undergraduate Teaching and Research Award

2015 Research at Brown Grant

2015 TERMIS SYIS-AM Undergraduate Travel Award

TEACHING EXPERIENCE

2016 Karen T. Romer Undergraduate Teaching and Research Award, updated the curriculum of the Tissue Engineering (BIOL 1140), Brown University

2015 Howard Hughes Medical Institute Summer Scholar Undergraduate Teaching Assistance, Genetics (BIOL 0470), Brown University

TRAINING

Laboratory: optical tissue clearing, immunohistochemistry, confocal microscopy, primary neural cell isolation, 3D cell culture, epifluorescent microscopy, mammalian tissue culture

Software: ImageJ/FIJI, Zen, Volocity, Adobe Illustrator and Photoshop, GraphPad Prism, Mendeley, Microsoft Office- Excel, Powerpoint and Word

ADDITIONAL RESEARCH EXPERIENCE

2014 National Center for Biodefense and Infectious Diseases, George Mason University, Manassass, VA.
Advisor: Ramin Hakami

Acknowledgments

I would like to start off by thanking Diane for giving me the opportunity to have such a positive research experience. Thank you for welcoming me to your lab 2 years ago and supporting me in my decision to do the concurrent degreed program. Thank you for always believing in me and for helping me develop as a scientist.

Thank you to my committee members Jackie Schell and Ulrike Mende, for their helpful advice and critiques of my experiments. A special thanks to Jackie for supported my degree program and keeping me up-to-date with all the relevant graduate emails.

I would like to thank all of the members of the Hoffman-Kim Lab for being such great people to work with. A huge thanks to Liane for being the nicest person I know and always checking up on me. Thank you for teaching me lab techniques and assisting me with experiments when I was overwhelmed. Samantha, thank you for being the best person I could ask for to work with. I loved working on the ischemia model with you. You made lab fun by being there for everything from brainstorming, planning experiments, and ranting about life. Thanks for exploring Providence with me, exploding bottles of media, and for your friendship. Best of luck next year and the years to come. And thank you to the rest of the Hoffman-Kim Lab: Lis, Matt, Jess, and Aurora, for your experimental advice and great conversations.

Thank you to the lab members who have since graduated. Thank you, Sam, for being my first mentor when I joined the lab and giving me an experience that made me want to stay for the next 2 years. Thanks for teaching me to be a good researcher from organizing data to planning experiments. Thank you, Molly, for being my role model and being patient answering all my constant questions. Thank you for all the hard work you've done in moving projects forward and giving me a place to pick up once you left.

Thank you to Jess Sadick from the Darling Lab and Nicolas Ledru from the Kaun Lab for helping me with RNA extraction and setting up qPCR. Thanks for answering questions, teaching me protocols, and lending your materials, equipment and time.

And finally, thank you to my parents and brother for inspiring me and pushing be to achieve my dreams. I wouldn't be here without your support.

Table of Contents

List of Figures

Chapter 1: The Formation and Dynamics of Capillary-Like Networks in Three-Dimensional Cortical Spheroids

1.1 Abstract

Central nervous system disease pathologies are poorly understood in part due to the inability of animal and *in vitro* models to recapitulate their complexity. It is therefore crucial to develop three-dimensional *in vitro* models of the central nervous system in which cells demonstrate more in-vivo-like gene and protein expression relative to traditional 2D culture. We previously described a primary cortical spheroid model that enables the *in vitro* study of *in vivo*-relevant characteristics, such as cell density, cell composition complexity, neuronal electrophysiology, tissue stiffness, and dimensionality. Importantly, cortical endothelial cells spontaneously assemble into capillary-like network structures within cortical spheroids, allowing for the study of the neurovasculature. Immunohistochemistry revealed that capillary-like networks are surrounded by basement membrane proteins and interact with relevant neural cell types. The networks are dynamic and change structure over the course of their lifetime, responding to the introduction of other cell types. This model provides a 3D scaffold-free environment to study interactions between the complex cells of the neurovascular unit in an *in vitro* setting. Additionally, the dysfunction of the neurovasculature in central

nervous system diseases makes this model applicable to investigating the vasculature in both healthy and diseased states.

1.2 Introduction

Diseases, disorders, and injuries of the central nervous system (CNS) are extremely prevalent and affect cognitive thinking, behavior, motility, and personality before ultimately resulting in death. The complex biological mechanisms involved in CNS disease pathologies are not well understood, resulting in slow development of new therapeutics. Also contributing to the prolonged nature of neuroscience therapeutic development is the inability of animal and *in vitro* models to recapitulate CNS diseases. Therefore, there is a need to create accurate *in vitro* models of the CNS in order to study pathologies and potential therapeutics (Hopkins, 2015). Engineering an *in vitro* model of the CNS is difficult due to the complex and intertwining arrangement of neurons, glia, neurovascular, and other involved cells. (Baker, 2012; Hopkins, 2015). *In vivo* cellular, biochemical, mechanical, and topographical cues create a microenvironment that influences critical cell behaviors such as viability, proliferation, differentiation, migration, and gene expression (Balgude, 2001; Bruder 2007; Li, 2007). However, traditional 2D cell culture models lack many of these environmental cues. The cells are cultured on surfaces that are orders of magnitude stiffer than *in vivo*, influencing cell behavior (Georges, 2006; Pampaloni, 2007). In addition, cells cultured in 2D take on a planar morphology without a three-dimensional

extracellular matrix (ECM) organization (Georges, 2006). These limitations aforementioned of traditional 2D cell culture models have spurred the creation of more comprehensive 3D *in vitro* models of the CNS.

3D *in vitro* models bridge the gap between traditional cultures and *in vivo* models as they provide an *in vivo*-like microenvironment while still being a tailorable experimental platform (Hopkins, 2015; Pampaloni, 2007). 3D *in vitro* models are created either with or without scaffolds. 3D models with scaffolds use artificial matrices to suspend the cells (Cullen, 2007; Irons, 2008; O'Shaughnessy, 2003). Scaffold-free techniques include self-assembly, in which the cells produce their own ECM (Choi, 2013; Kato-Negishi, 2013). Recent studies suggest that 3D self-assembled neural cultures approximate *in vivo*-like cell behavior better than 2D or scaffold-based 3D cell cultures (Fennema, 2013; Lin, 2008).

Our lab has used a technique to generate 3D scaffold-free spheroids from primary postnatal rat cortical cells that are reproducible in size and characteristics. This spheroid model enables the *in vitro* study of *in vivo*-relevant characteristics, such as cell density, cell composition complexity, neuronal electrophysiology, tissue stiffness, and dimensionality (Dingle, 2015). In addition, our spheroids contain endothelial cells that spontaneously form networks without exogenously introduced vasculogenic growth factors

surrounded by a laminin, collagen type IV, and fibronectin ECM. These capillary-like networks were seen to form lumens and tight junctions. (Boutin, 2017).

The presence of capillary-like networks (CLNs) in our cortical spheroids allows for the study of the neurovasculature. Neurovascular dysfunction is linked to many CNS diseases – namely, stroke, traumatic brain injury, and Alzheimer's Disease – which, makes the understanding of the neurovasculature and its dysfunction essential for the development of therapeutics.

The neurovasculature in the CNS includes the blood-brain barrier (BBB), a highly selective permeable membrane that separates the circulating blood from the CNS (Daneman, 2010). It functions as a physical barrier, transport barrier, and metabolic barrier to provide a stable fluid microenvironment that is critical for complex neural function and protects the CNS from chemical insult and damage (Abbott, 2010). The BBB is a complex microvascular system composed of different specialized cell types including endothelial cells, pericytes, and astrocytes. Together with the neurons, these three cell types form what is termed the neurovascular unit (Urich, 2013). The basement membrane of the BBB mostly is made up of structural proteins

such as collagen type IV, laminin, and fibronectin, and also contains cell adhesion molecules and immobilized signaling proteins (Obermeier, 2013).

The selectivity of the BBB is maintained by the specialized endothelial cells (ECs) that form the lumen of the capillaries (Abbott, 2010). Endothelial cells in the brain are distinct from ECs found throughout the majority of the body due to their restrictive properties (Calabria, 2008). First, elaborate tight junctions stitch adjacent endothelial cells together and prevent soluble blood-borne materials from crossing between the cells. Second, CNS endothelial cells have extremely low rates of transcytosis compared to endothelial cells in other organs (Hagan, 2015). Together, this limits movement of molecules through the BBB and makes molecular transport dependent on specific transporters.

The unique properties of the CNS ECs are not intrinsic but rather induced by other neural cells (Daneman, 2010). Pericytes ensheath the abluminal surfaces of cerebral vessel walls including those of capillaries, precapillary arterioles and postcapillary venules (Obermeier, 2013) They form direct contacts with the endothelium through N-cadherin and connexins, allowing exchanges of ions, metabolites, second messengers, and ribonucleic acids between the two cell types (Zhao, 2015). Pericytes are necessary for the formation and integrity maintenance of the BBB (Daneman, 2010; Eichmann,

2013; Engelhart, 2003; Obermeier, 2013; Vallon, 2014). Roles played by the pericytes include aiding the formation of tight junctions, aiding in angiogenesis and microvascular stability, regulating vesicle trafficking and gene expression patterns in the ECs, and regulating capillary diameter and blood flow (Daneman, 2010; Girouard, 2006; Hagan, 2015, Urich, 2013; Zhao, 2015).

Astrocytes and their precursors have also been implicated in the induction of BBB properties (Engelhart, 2003). The astrocyte is a CNS specific glial cell type that wraps its distal processes, or astrocytic endfeet, around the outer surface of the capillaries (Hagan, 2015). The endfeet are highly polarized and rich in the water channel aquaporin-4 that regulates electrolyte and water balance (Obermeier, 2013; Prakash, 2015). Co-culture models have shown that compared with ECs cultured alone, ECs co-cultured with astrocytes exhibit improved barrier functions (Obermeier, 2013; Prakash, 2015).

The development of the BBB is a multistep process that begins with angiogenesis when preexisting vessels sprout into the embryonic neuroectoderm and give rise to new vessels (Obermeier, 2013). Vessels elongate, produce manifold branches and finally anastomose with adjacent sprouts to form a plexus of undifferentiated capillaries in the ventricular zone of the developing brain (Engelhart, 2003). The Wnt signaling pathway is

activated in CNS ECs during embryogenesis and has been identified as an essential regulator of developmental CNS angiogenesis and BBB formation (Obermeier, 2013; Vallon, 2014). Activation of Wnt signaling leads to the induction of genes critical for the BBB formation, such as glucose transporter Glut1 and death receptors DR6 and TROY (Zhao, 2015). It is debatable whether humans and/or other mammals are born with a fully functional BBB (Zhao, 2015) or if many of the characteristics of the BBB transport mechanisms continue to mature in the peri- and post-natal periods (Abbott, 2010). Barrier maturation is regulated by the Hedgehog pathway (Obermeier, 2013). A study of cerebral microvascular plasticity in mice found large-scale sprouting and pruning of microvessels in the first post-natal month. In the adult brain, the net number of vessels had stabilized although there was some vessel formation and elimination throughout life (Harb, 2013).

There are a variety of ways in which researchers have modeled the BBB *in vitro*. 2D *in vitro* BBB models are suboptimal because the brain endothelial cells dedifferentiate spontaneously and lose BBB properties. A common 2D *in vitro* model is a monolayer of brain endothelial cells grown on a porous membrane, effectively dividing the culture chamber into two compartments representing the blood and brain (Calabria, 2008). Meanwhile, 3D models are able to provide the three-dimensional cellular organization required for proper cellular differentiation (Urich, 2013). The most widely used systems

for culturing endothelial cells in 3D are Matrigel, collagen gels, or mixed ECM gels where the endothelial cells grow and differentiate to form loose network-like structures (Kunz-Schughart, 2005). Several *in vitro* BBB models co-culture cerebral brain endothelial cells with primary glial cells to mimic the *in vivo* BBB microenvironment (Engelhart, 2003). A study in 2013 used a 3D spheroid culture to model the BBB by co-culturing primary brain endothelial cells, primary pericytes, and primary astrocytes, and allowing them to spontaneously self-organize into a spheroid structure that recapitulates the complex arrangement of the individual cell types in the BBB structure (Urich, 2013). However, this model does not fully recapitulate the neurovascular unit as it does not include neurons.

In the present study, our goal was to further characterize the structure and dynamics of self-assembling capillary-like networks in cortical spheroids. The spheroids contain many neural cell types including neurons, astrocytes, neural stem cells, microglia, and oligodendrocytes as well as the endothelial cells composing the networks. Capillary-like networks are surrounded by basement membrane proteins, and interact with relevant neural cell types. The networks are dynamic and change their structure over the course of their lifetime and respond to the introduction of other cell types. This model provides a 3D scaffold-free environment to study interactions between the complex cells of the neurovascular unit in an *in vitro* setting.

1.3 Methods

1.3.1 Cell culture

Cortical Cells

Primary cortical tissues were dissected from postnatal day 1-3 rats. The cell isolation protocol was modified from BrainBits, LLC. Tissues were cut into small pieces and digested in papain solution (2 mg/mL of papain in Hibernate A without calcium) for 30 min at 30°C. Papain solution was removed and replaced with a Hibernate A buffer solution (Hibernate A supplemented with 0.5 mM Glutamax and 1x B27 growth supplement). The tissues were triturated with a fire polished pasteur pipette and centrifuged at 150 xg for 5 min. The supernatant was removed, the cell pellet was re-suspended in Neurobasal A media, and the cell solution was passed through a 40 μm cell strainer to remove debris. The cell solution was once again centrifuged at 150 xg for 5 min, re-suspended in Neurobasal A media, and strained. Cell viability was determined at the time of isolation by a trypan blue exclusion assay. Finally, cells were seeded directly into 3D microtissues or onto cell culture plates coated with poly-d-lysine. Cortical neurons were maintained in Neurobasal-A media with 1% penicillin/streptomycin, 0.5 mM Glutamax, and 1x B27 growth supplement with media changes every 3-4 days.

Fibroblasts

NIH 3T3 cells were cultured in Dulbecco's Modified Eagle's Medium with 1% penicillin/streptomycin and 10% fetal bovine serum. Cell media was changed every 3-4 days.

1.3.2 3D self-assembled spheroid fabrication

Scaffold-free microtissue spheres were made using agarose gels with 96 spherical microwells. 2% molten agarose was poured onto the spheroid micromold with 400 μm diameter round pegs from Microtissues, Inc. This resulted in agarose gels with round-bottomed microwells. Agarose gels were equilibrated in cell culture media with three media changes over 48 hours. Cell solution containing the appropriate number of cells was centrifuged and re-suspended in media. The media from the agarose gels was aspirated, and 75 μL of the cell solution was seeded in the agarose gels. Cells were allowed to settle into the microwells for 45 min, and 1 mL of media was added.

1.3.3 Whole spheroid immunostaining and optical clearing

Spheroids were fixed in 4% v/v paraformaldehyde and 8% w/v sucrose in phosphate-buffered saline (PBS) overnight, followed by three 30 min PBS washes. All of the following steps were performed on a shaker at room temperature. Spheroids were permeabilized and blocked with 10% normal goat serum, 4% bovine serum albumin, and 1% Triton X-100 in PBS for 2 hours, and subsequently incubated in primary antibody diluted in blocking solution overnight. The following day, the spheroids underwent two 2 hour washes in 0.2% Triton X-100 in PBS followed by 2 hour blocking in blocking solution. Spheroids were incubated in secondary antibody diluted in blocking solution overnight. The following day, the spheroids underwent three 30 min

washes in 0.2% Triton X-100 in PBS and incubated in 1µg/mL of 4',6-diamidino-2-phenylindole (DAPI) in PBT for 1 hr and returned to PBS.

The ClearT2 solutions and protocol were used for optical clearing (Boutin, 2014). Briefly, spheres were incubated in: 1) 25% formamide/10% poly-ethylene glycol (PEG) for 10 min, 2) 50% formamide/20% PEG for 5 min, and 3) 50% formamide/20% PEG for 60 min. Spheroids were kept in final clearing solution and transferred to glass-bottom confocal dishes for imaging on a Zeiss LSM 510 Meta Confocal Laser Scanning Microscope.

1.3.4 Spheroids cryosectioning and immunostaining

Spheroids were fixed in 4% v/v paraformaldehyde and 8% w/v sucrose in phosphate-buffered saline (PBS) overnight, followed by three 30 min PBS washes. Whole agarose gels with fixed spheroids were incubated in 15% wt/vol sucrose in PBS for 3 hours, followed by 3 hours in 30% wt/vol sucrose in PBS. Agarose gels were then blotted dry and embedded in O.C.T. compound. Blocks were stored at -80°C until cryosectioning on a Leica CM3050 S Cryostat. Sections were cut at a thickness of 8 µm onto SuperFrost Plus slides.

Sections were then fixed in 4% vol/vol paraformaldehyde with 8% wt/vol sucrose in PBS for 10 min and washed twice with PBS. Sections were permeabilized with PBT for 15 min, washed twice with PBS, and blocked

with 10% normal goat serum, 4% bovine serum albumin, and 1% Triton X-100 in PBS for 1 hour. Sections were incubated overnight at 4°C in a humidified chamber with primary antibody diluted in PBS. Sections underwent two 30 min washes in PBT, followed by a 30 min wash in PBS. Sections were incubated in secondary antibody diluted in blocking solution for 1 hour at room temperature and subsequently washed two times in PBT for 10 min each. DAPI counterstaining was performed for 10 min, followed by two PBS washes. Sections were mounted with Fluoromount-G and imaged on a Zeiss LSM 510 Meta Confocal Laser Scanning Microscope.

Antibody	Dilution	Company Catalog #
Primary Antibodies		
Rabbit polyclonal anti-laminin	1:100	BTI BT-594
Rabbit polyclonal anti-vWF	1:50	Dako A0082
Chicken polyclonal anti-GFAP	1:500	Dako Z0334
Mouse monoclonal anti-pan Cadherin	1:50	Abcam ab6528
Secondary Antibodies		
Cy3 goat anti-rabbit	1:500 (sections) 1:200 (spheroids)	Jackson 111-165-144
Alexa Fluor 488 goat anti-mouse	1:500	Jackson 115-545-146
Alexa Fluor 633 goat anti-chicken	1:200	ThermoFischer A-21103
Alexa Fluor 647 goat anti-rabbit	1:200	Jackson 111-605-144

1.3.5 Cortical and fibroblast spheroid fusion

Dissociated cortical cells and fibroblasts were labelled with CellTracker Red or Green respectively prior to being seeded into spheroids. CellTracker dyes of 10 mM in DMSO were diluted in cell media to a final concentration of 2.5

μM. Cells were incubated in the dye for 20 min at 37°C. The cells were centrifuged, the dye was removed, and the cells were rinsed in fresh media for 10 min at room temperature. Cortical cells were stained with CellTracker Red and seeded into 8,000 cell spheroids. NIH 3T3 fibroblasts were stained with CellTracker Green and seeded into 3,000 cell spheroids. Day 3 cortical spheroids and Day 2 fibroblast spheroids were fused by inverting one gel on top of the other and centrifuging for 1 min at 150G to pull the spheroids into the lower wells. The fused spheroids were maintained in complete cortical media, live imaged daily, and fixed after 2 or 4 days. Samples were stained for laminin and imaged using confocal microscopy.

1.4 Results

1.4.1 Capillary-like networks interacted with relevant neural cell types

Cortical tissue of postnatal day 1-2 rat pups was dissected, dissociated, and the cells were seeded into non-adhesive microwells, which promoted cellular self-assembly into 3D scaffold-free spheroids. Cultures were maintained in neuronal growth medium containing the neuronal supplement B27, which does not contain vasculogenic growth factors. As previously described, the cortical spheroids contained endothelial cells that spontaneously formed networks surrounded by ECM proteins. These capillary-like networks were seen to form lumens and tight junctions. (Boutin, 2017).

The neurovascular environment in the brain is complex and requires diverse cell types to form the blood-brain barrier (Obermeier, 2013). As previously described, cortical spheroids contain these diverse cell types, including neurons, astrocytes, oligodendrocytes, neural progenitor cells, and microglia (Dingle, 2015). Yet in order to effectively model the complexity of the neurovascular environment, an *in vitro* model must have interactions between these neural cell types.

Glial fibrillary acidic protein (GFAP)-positive astrocytes, which *in vivo* extend endfeet around mature neurovasculature, were present in the cortical spheroids and formed extensions adjacent to capillary-like networks. Additionally, cadherin adherens junction proteins were present, showing cell-cell adhesion and suggesting the formation of functional interactions (Figure 1.1) (Halbleib, 2006).

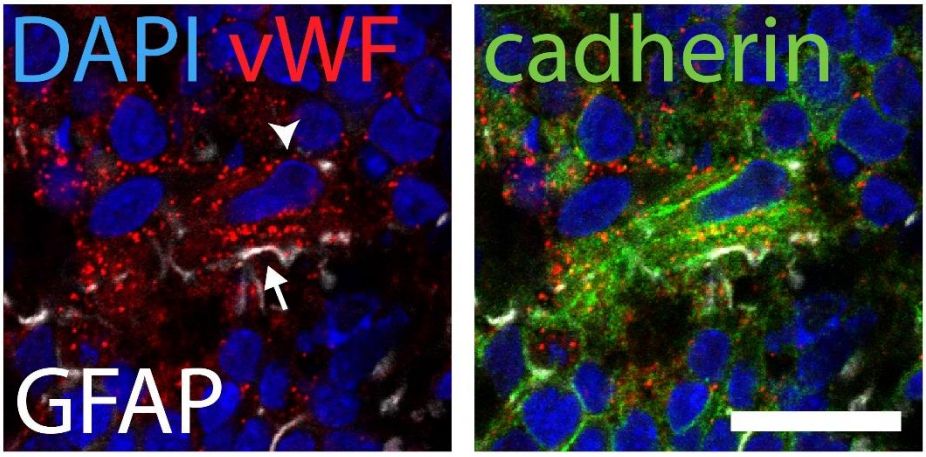

Figure 1.1 Single z-slice image of cryosection stained for DAPI (blue, arrowhead highlights elongated nucleus), vWF (red), GFAP (white, arrow highlights extension adjacent to network), and pan-cadherin (green). Scale bar, 20μm

1.4.2 Capillary-like networks are dynamic structures that developed over time

To observe the development of capillary-like networks, immunohistochemistry for laminin (Ln) was performed. Ln is a well-established biomarker for neural vasculature (Hutter-Schmid, 2015). After 1 DIV (day *in vitro*) in culture, dense, disconnected, Ln-positive nodules were observed throughout the spheroid (Figure 1.2). At 3 DIV, dense foci were less common and were replaced by extended Ln-positive tubular structures, typically found within the spheroid center. To estimate the frequency with which these networks formed, approximately 140 spheroids were examined per time point for three independent experiments. The number of spheroids with Ln-positive network structures, out of total spheroids counted, was 70% at 3 DIV (Figure 1.3). Network structures decreased in both size and frequency until they were absent in 14 and 21 day-old spheroids. Instead of tubular network structures, 14 and 21 day-old spheroids had single, dense Ln-positive nodules in the center of the spheroid (Figure 1.2).

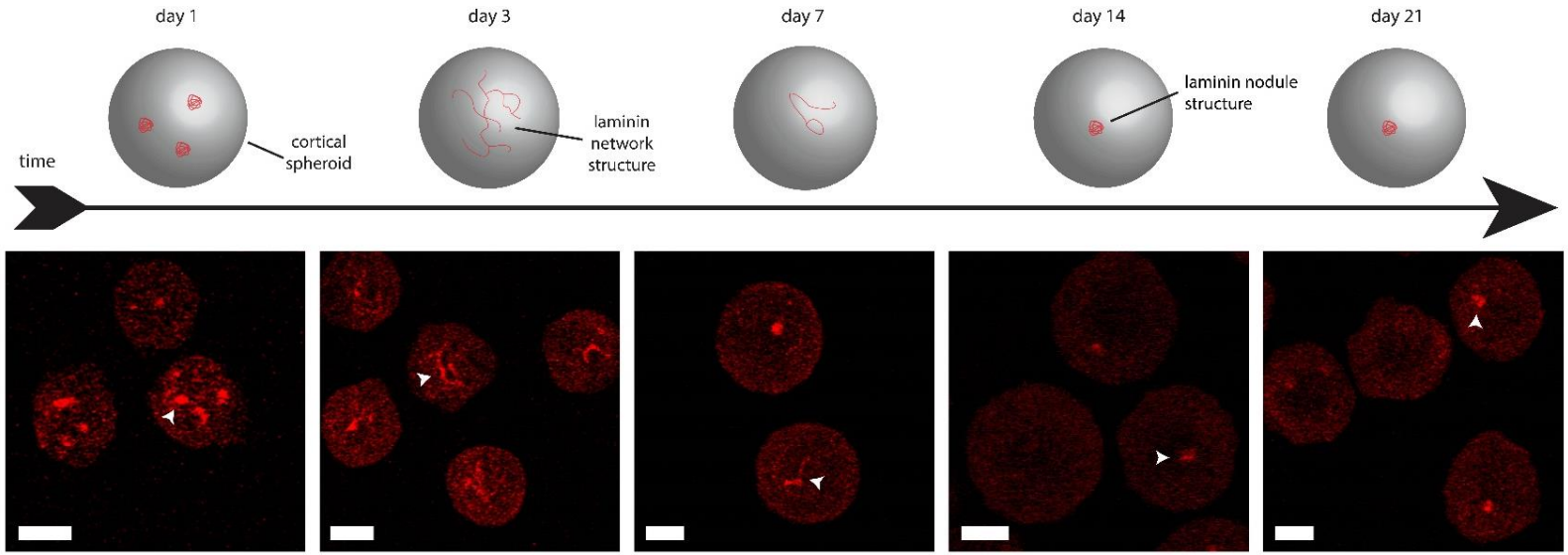

Figure 1.2 Experimental design cartoon and confocal z-slice projection of spheroids stained for Ln (red, arrowheads highlight Ln features) at 1, 3, 7, 14, and 21 DIV. Scale bar, 100 μm

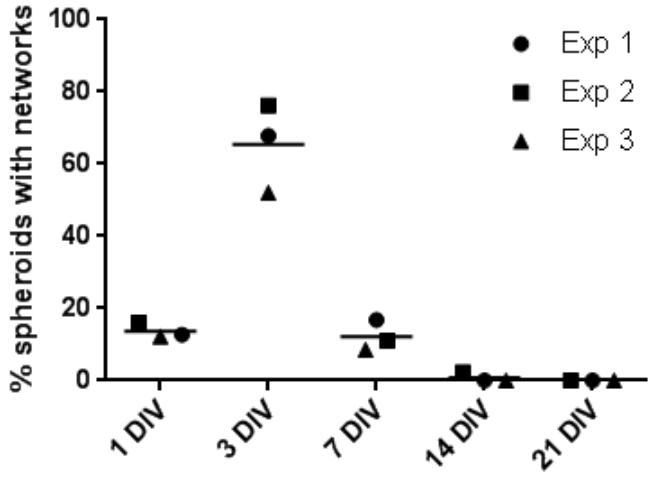

Figure 1.3 Graph of percent of spheroids with capillary-like networks for three independent experiments. Horizontal line depicts mean for each time point.

1.4.3 Endothelial cells composing the CLNs migrated toward added fibroblasts

In order to better understand the environmental factors that contribute to capillary-like network formation and breakdown, NIH 3T3 fibroblast spheroids were fused with cortical spheroids. Endothelial cells are often co-cultured with fibroblasts in spheroids in *in vitro* models of angiogenesis. (Eckermann, 2011; Kunz-Schughart, 2005).

Fused cortical-NIH 3T3 spheroids integrated after 2 days, retaining a clear interfacial border. After 3 days, the CTgreen labeled NIH 3T3 spheroid began to lose its spheroid shape and integrate with the CTred labeled cortical

spheroid (Figure 1.4). Cell tracker staining of the cortical cells was unable to distinguish individual cortical cells. Shortening the experiment length by fusing the spheroids for 2 fewer days in order to reduce loss of the fluorescent label did little to improve the cortical labeling.

Diffuse Ln staining was observed throughout the fused spheroids, with increased Ln staining in the NIH 3T3 region. No Ln-labeled CLNs were observed within the cortical region. However, network structures were observed within NIH 3T3 regions. These structures were recognized by the presence of elongated nuclei within the NIH 3T3 microtissue region that were bordered by increased Ln staining (Figure 1.5). The elongated nuclei appeared to be CTgreen-negative however the poor CTred labeling did not allow us to confirm that they were CTred-positive cells. We hypothesize that these cells represent cortical ECs that have migrated into the NIH 3T3 spheroid region.

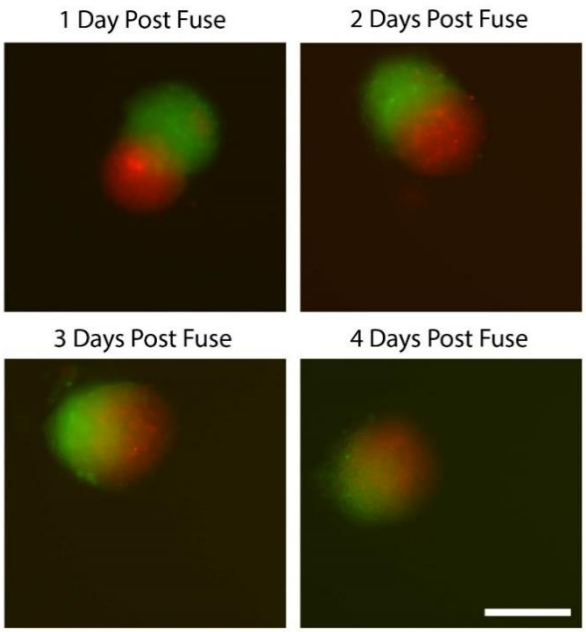

Figure 1.4 Epifluorescent images of postnatal rat cortical spheroid (CellTracker Red) fusing with NIH 3T3 spheroid (CellTracker Green) over the course of four days. Scale bar, 200µm

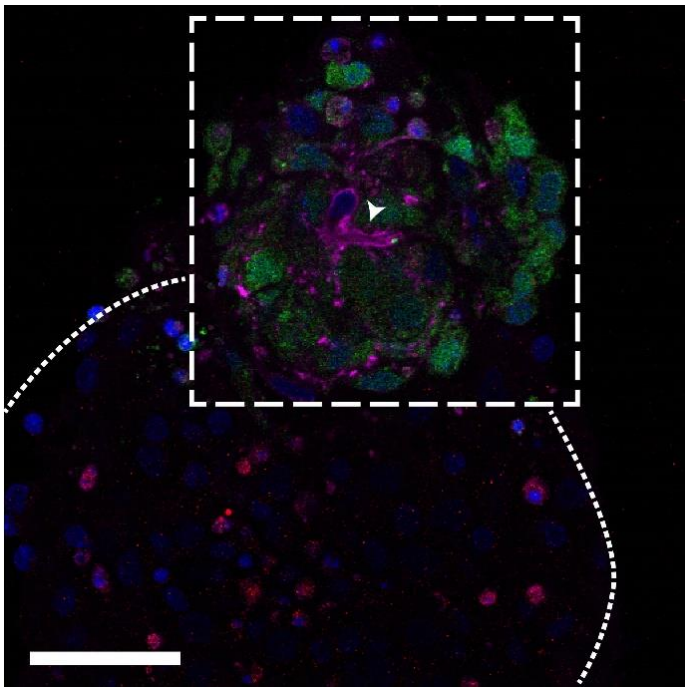

Figure 1.5 Confocal z-stack projection of postnatal rat cortical spheroid labeled with CellTracker Red, co-cultured with NIH 3T3 spheroid labeled with CellTracker Green. Ln, pink (arrow highlights network structure). Dashed box encloses NIH 3T3 spheroid, dotted line outlines edges of rat cortical spheroid. Scale bar, 50µm

1.5 Discussion

We have further characterized the formation of CLNs in our cortical spheroid model. The endothelial cells composing the networks form lumens and are surrounded by a basement membrane of laminin, collagen type IV, and fibronectin. The networks interact with other neural cells such as astrocytes as suggested by the presence of cadherin adherens junction proteins. Interactions with relevant neural cells further suggests that the CLNs have properties of the BBB as it is the neural cells that induce the unique properties of the CNS endothelial cells (Daneman, 2010).

This *in vitro* model of the neurovasculature allows for higher throughput studies because of the number of spheroids that can be formed. Gel molds allow for 96 spheroids to be made per well in a 24-well plate and each gel model makes approximately 62 network-containing spheroids. It is possible to study many spheroids for a given experimental condition using this model.

However, the short life span of the CLNs currently only permits studies of the networks at a certain age. Networks are well formed and most extensive after 3 days yet condense into laminin-rich nodules by 14 days. In future experiments it will be interesting to investigate the formation of Ln-rich nodules in cortical spheroids, including the cells and dynamics involved. A possible reason for the loss of the networks could be the lack of intravascular fluid flow. In ECs, shear stresses activate intracellular signaling cascades

that affect processes from cell proliferation to migration, and alter EC protein expression (Li, 2005). The dynamics of CLN formation, maintenance, breakdown, and condensation into nodules can be studied further using endogenously labeled ECs, perhaps using cortical spheroids from Tie2-reporter mice. Endogenously labeled ECs will allow for real-time imaging of the network dynamics.

The complexity of cortical EC CLN formation was further revealed through the NIH-3T3-cortical spheroid fusion experiment. In NIH 3T3-cortical fused spheroids no Ln-labeled CLNs were present within cortical spheroid regions. Instead, networks were observed within NIH 3T3 spheroid regions. Fibroblasts are known to support and modulate EC migration, viability, and network formation in 3D tissue-like environments (Kunz-Schughart, 2005). It is believed that fibroblast-derived extracellular matrix components play a role in supporting lumen formation (Newman, 2011). We therefore hypothesize that cortical ECs migrate to favorable microenvironments in the NIH 3T3 spheroid regions with increased supportive ECM content and vasculogenic growth factor production. Due to the poor CTred staining future experiments will need to confirm that cortical ECs do in fact form the network structures—possibly through the use of endogenously labeled ECs. In future experiments it will be interesting to see if the culture of cortical spheroids in fibroblast conditioned media or in growth factors such as VEGF,

FGF-2, and EGF will similarly influence the CLNs. Forthcoming studies will also involve studying the response of cortical CLNs to other various introduced cell types including peripheral immune cells and brain cancer cell lines to inform EC responses to CNS disease states.

1.6 References

Abbott, N. J., Patabendige, A. A. K., Dolman, D. E. M., Yusof, S. R., & Begley, D. J. (2010). Structure and function of the blood–brain barrier. *Neurobiology of Disease*, *37*(1), 13–25. http://doi.org/10.1016/j.nbd.2009.07.030

Baker, B. M., & Chen, C. S. (2012). Deconstructing the third dimension - how 3D culture microenvironments alter cellular cues. *Journal of Cell Science*, *125*(13), 3015–3024. http://doi.org/10.1242/jcs.079509

Balgude, A. P., Yu, X., Szymanski, A., & Bellamkonda, R. V. (2001). Agarose gel stiffness determines rate of DRG neurite extension in 3D cultures. *Biomaterials*, *22*(10), 1077–84. Retrieved from http://www.ncbi.nlm.nih.gov/pubmed/11352088

Boutin, M. E., Kramer, L. L., Livi, L. L., Brown, T., Moore, C., & Hoffman-Kim, D. (2017). A three-dimensional neural spheroid model for capillary-like network formation. *Journal of Neuroscience Methods*. http://doi.org/10.1016/j.jneumeth.2017.01.014

Bruder, J. M., Lee, A. P., & Hoffman-Kim, D. (2007). Biomimetic materials replicating Schwann cell topography enhance neuronal adhesion and neurite alignment in vitro. *Journal of Biomaterials Science, Polymer Edition*, *18*(8), 967–982. http://doi.org/10.1163/156856207781494412

Calabria, A. R., & Shusta, E. V. (2008). A Genomic Comparison of *in vivo* and *in vitro* Brain Microvascular Endothelial Cells. *Journal of Cerebral Blood Flow & Metabolism*, *28*(1), 135–148. http://doi.org/10.1038/sj.jcbfm.9600518

Choi, Y. J., Park, J., & Lee, S.-H. (2013). Size-controllable networked neurospheres as a 3D neuronal tissue model for Alzheimer's disease studies. *Biomaterials*, *34*(12), 2938–2946. http://doi.org/10.1016/j.biomaterials.2013.01.038

Cullen, D. K., Stabenfeldt, S. E., Simon, C. M., Tate, C. C., & LaPlaca, M. C. (2007). In vitro neural injury model for optimization of tissue-engineered constructs. *Journal of Neuroscience Research*, *85*(16), 3642–3651. http://doi.org/10.1002/jnr.21434

Daneman, R., Zhou, L., Kebede, A. A., & Barres, B. A. (2010). Pericytes are required for blood–brain barrier integrity during embryogenesis. *Nature*, *468*(7323), 562–566. http://doi.org/10.1038/nature09513

Dingle, Y.-T. L., Boutin, M. E., Chirila, A. M., Livi, L. L., Labriola, N. R., Jakubek, L. M., … Hoffman-Kim, D. (2015). Three-Dimensional Neural Spheroid Culture: An In Vitro Model for Cortical Studies. *Tissue Engineering. Part C, Methods*, *21*(12), 1274–83. http://doi.org/10.1089/ten.TEC.2015.0135

Eckermann, C. W., Lehle, K., Schmid, S. A., Wheatley, D. N., & Kunz-Schughart, L. A. (2011). Characterization and modulation of fibroblast/endothelial cell co-cultures for the *in vitro* preformation of three-dimensional tubular networks. *Cell Biology International*, *35*(11), 1097–1110. http://doi.org/10.1042/CBI20100718

Eichmann, A., & Thomas, J.-L. (2013). Molecular Parallels between Neural and Vascular Development. *Cold Spring Harbor Perspectives in Medicine*, *3*(1), a006551–a006551. http://doi.org/10.1101/cshperspect.a006551

Engelhardt, B. (2003). Development of the blood-brain barrier. *Cell and Tissue Research*, *314*(1), 119–129. http://doi.org/10.1007/s00441-003-0751-z

Fennema, E., Rivron, N., Rouwkema, J., van Blitterswijk, C., & de Boer, J. (2013). Spheroid culture as a tool for creating 3D complex tissues. *Trends in Biotechnology*, *31*(2), 108–115. http://doi.org/10.1016/j.tibtech.2012.12.003

Georges, P. C., Miller, W. J., Meaney, D. F., Sawyer, E. S., & Janmey, P. A. (2006). Matrices with Compliance Comparable to that of Brain Tissue Select Neuronal over Glial Growth in Mixed Cortical Cultures. *Biophysical Journal*, *90*(8), 3012–3018. http://doi.org/10.1529/biophysj.105.073114

Girouard, H., & Iadecola, C. (2006). Neurovascular coupling in the normal brain and in hypertension, stroke, and Alzheimer disease. *Journal of Applied Physiology*, *100*(1), 328–335. http://doi.org/10.1152/japplphysiol.00966.2005

Hagan, N., & Ben-Zvi, A. (2015). The molecular, cellular, and morphological components of blood–brain barrier development during embryogenesis. *Seminars in Cell & Developmental Biology*, *38*, 7–15. http://doi.org/10.1016/j.semcdb.2014.12.006

Halbleib, J. M., & Nelson, W. J. (2006). Cadherins in development: cell adhesion, sorting, and tissue morphogenesis. *Genes & Development*, *20*(23), 3199–3214. http://doi.org/10.1101/gad.1486806

Harb, R., Whiteus, C., Freitas, C., & Grutzendler, J. (2013). *In Vivo* Imaging of Cerebral Microvascular Plasticity from Birth to Death. *Journal of Cerebral Blood Flow & Metabolism*, *33*(1), 146–156. http://doi.org/10.1038/jcbfm.2012.152

Hopkins, A. M., DeSimone, E., Chwalek, K., & Kaplan, D. L. (2015). 3D in vitro modeling of the central nervous system. *Progress in Neurobiology*, *125*, 1–25. http://doi.org/10.1016/j.pneurobio.2014.11.003

Hutter-Schmid, B., Kniewallner, K. M., & Humpel, C. (2015). Organotypic brain slice cultures as a model to study angiogenesis of brain vessels. *Frontiers in Cell and Developmental Biology*, *3*, 52. http://doi.org/10.3389/fcell.2015.00052

Irons, H. R., Cullen, D. K., Shapiro, N. P., Lambert, N. A., Lee, R. H., & LaPlaca, M. C. (2008). Three-dimensional neural constructs: a novel platform for neurophysiological investigation. *Journal of Neural Engineering*, *5*(3), 333–341. http://doi.org/10.1088/1741-2560/5/3/006

Kato-Negishi, M., Morimoto, Y., Onoe, H., & Takeuchi, S. (2013). Millimeter-Sized Neural Building Blocks for 3D Heterogeneous Neural Network Assembly. *Advanced Healthcare Materials*, *2*(12), 1564–1570. http://doi.org/10.1002/adhm.201300052

Kunz-Schughart, L. A., Schroeder, J. A., Wondrak, M., van Rey, F., Lehle, K., Hofstaedter, F., & Wheatley, D. N. (2005). Potential of fibroblasts to regulate the formation of three-dimensional vessel-like structures from endothelial cells in vitro. *AJP: Cell Physiology*, *290*(5), C1385–C1398. http://doi.org/10.1152/ajpcell.00248.2005

Li, G. N., Livi, L. L., Gourd, C. M., Deweerd, E. S., & Hoffman-Kim, D. (2007). Genomic and Morphological Changes of Neuroblastoma Cells in Response to Three-Dimensional Matrices. *Tissue Engineering*, *13*(5), 1035–1047. http://doi.org/10.1089/ten.2006.0251

Li, Y. J., Haga, J. H., & Chien, S. (2005). Molecular basis of the effects of shear stress on vascular endothelial cells. *Journal of Biomechanics*, *38*, 1949–1971. http://doi.org/10.1016/j.jbiomech.2004.09.030

Lin, R.-Z., Chang, H.-Y., & Chang, H.-Y. (2008). Recent advances in three-dimensional multicellular spheroid culture for biomedical research. *Biotechnology Journal*, *3*(9–10), 1172–1184. http://doi.org/10.1002/biot.200700228

Newman, A. C., Nakatsu, M. N., Chou, W., Gershon, P. D., & Hughes, C. C. W. (2011). The requirement for fibroblasts in angiogenesis: fibroblast-derived matrix proteins are essential for endothelial cell lumen formation. *Molecular Biology of the Cell*, *22*(20), 3791–800. http://doi.org/10.1091/mbc.E11-05-0393

O'Shaughnessy, T. J., Lin, H. J., & Ma, W. (2003). Functional synapse formation among rat cortical neurons grown on three-dimensional collagen gels. *Neuroscience Letters*, *340*(3), 169–72. Retrieved from http://www.ncbi.nlm.nih.gov/pubmed/12672533

Obermeier, B., Daneman, R., & Ransohoff, R. M. (2013). Development, maintenance and disruption of the blood-brain barrier. *Nature Medicine*, *19*(12), 1584–1596. http://doi.org/10.1038/nm.3407

Pampaloni, F., Reynaud, E. G., & Stelzer, E. H. K. (2007). The third dimension bridges the gap between cell culture and live tissue. *Nature Reviews Molecular Cell Biology*, *8*(10), 839–845. http://doi.org/10.1038/nrm2236

Prakash, R., & Carmichael, S. T. (2015). Blood–brain barrier breakdown and neovascularization processes after stroke and traumatic brain injury. *Current Opinion in Neurology*, *28*(6), 556–564. http://doi.org/10.1097/WCO.0000000000000248

Urich, E., Patsch, C., Aigner, S., Graf, M., Iacone, R., & Freskgård, P.-O. (2013). Multicellular Self-Assembled Spheroidal Model of the Blood Brain Barrier. *Scientific Reports*, *3*, 1500. http://doi.org/10.1038/srep01500

Vallon, M., Chang, J., Zhang, H., & Kuo, C. J. (2014). Developmental and pathological angiogenesis in the central nervous system. *Cellular and Molecular Life Sciences*, *71*(18), 3489–3506. http://doi.org/10.1007/s00018-014-1625-0

Zhao, Z., Nelson, A. R., Betsholtz, C., & Zlokovic, B. V. (2015). Establishment and Dysfunction of the Blood-Brain Barrier. *Cell*, *163*(5), 1064–1078. http://doi.org/10.1016/j.cell.2015.10.067

Chapter 2: Optimization of the Lactate Dehydrogenase Cell Viability Assay for Use in Three-Dimensional Cortical Spheroids

2.1 Abstract

As 3D cell culture methods are developed and become more widely used, it is essential that compatible assays are simultaneously developed. Almost all assays that have been developed to analyze the qualities of cells in culture have only been tested and optimized for conventional 2D culture. We optimized the lactate dehydrogenase assay, a common cell viability assay, for our three-dimensional cortical spheroids. We prepared serial dilutions of cells in 2D and spheroids of varying sizes to find the cell number for which LDH release is linear, a condition required for optimal results. We have confirmed that the LDH release assay can be used for cortical spheroids. This provides the potential for using the LDH assay in conjunction with cortical spheroids for disease and injury models of the central nervous system.

2.2 Introduction

Traditionally, *in vitro* cell culture has meant culture in two dimensions on treated tissue culture plates. Almost all assays that have been developed to test the qualities of cells in culture have only been tested and optimized for conventional 2D culture. In order for 3D *in vitro* cell culture to become a widely accessible and utilized technique, there needs to be a wide variety of

assays that can be used. Assays optimized for two dimensions cannot necessarily be applied in three dimensions. For example, 3D cultures require that reagents diffuse longer distances and it can therefore be expected that assays using reagents may require a higher concentration of reagent and a longer incubation time.

A common assay for cell viability is the lactate dehydrogenase release assay. Lactate dehydrogenase (LDH) is a cytosolic enzyme present in many different cell types and responsible for catalyzing the conversion of lactate to pyruvic acid and back. Plasma membrane damage releases LDH into the cell media, making it a compound that can be quantified to determine viability. Extracellular LDH can be quantified using a coupled enzymatic reaction in which LDH catalyzes the conversion of lactate to pyruvate via NAD+ reduction to NADH. Diaphorase then uses NADH to reduce a tetrazolium salt to a red formazan product that can be measured at 490nm. The level of formazan formation is directly proportional to the amount of LDH released into the medium, which is indicative of cytotoxicity (Pierce LDH assay manual).

The LDH release assay is very commonly used in cytotoxicity studies including 2D *in vitro* models of ischemia (Li, 2008; Lyons, 1998; Ohmori, 1996; Ruscher, 2002; Xu, 2001). Although originally developed for 2D cell

cultures, it is a common assay for cytotoxicity of cells grown in spheroids (Ho, 2012). Studies that use an LDH release assay in spheroids tend to use the same manufacturer's protocol for both 2D and spheroid cultures (Ho, 2012; Lee, 2009). However, to our knowledge, the LDH release assay has yet to be used in spheroid models of ischemia.

In the present study, our goal was to confirm that the LDH release assay can be used to assess viability of our primary postnatal rat cortical spheroids. Optimal results from the LDH release assay requires that the number of cells used corresponds to LDH release within a linear range. We prepared serial dilutions of cells in 2D and spheroids of varying sizes to find the cell number for which LDH release is linear. We have confirmed that the LDH release assay can be used for cortical spheroids.

2.3 Methods

2.3.1 Cell culture

Primary cortical tissues were dissected from postnatal day 1-3 rats. The cell isolation protocol was modified from BrainBits. Tissues were cut into small pieces and digested in papain solution (2 mg/mL of papain in Hibernate A without calcium) for 30 min at 30°C. Papain solution was removed and replaced with a Hibernate A buffer solution (Hibernate A supplemented with 0.5 mM Glutamax and 1x B27 growth supplement). The tissues were triturated with a fire polished pasteur pipette and centrifuged at 150 xg for 5

min. The supernatant was removed, the cell pellet was re-suspended in Neurobasal A media, and the cell solution was passed through a 40 μm cell strainer to remove debris. The cell solution was once again centrifuged at 150 xG for 5 min, re-suspended in Neurobasal A media, and strained. Cell viability was determined at the time of isolation by a trypan blue exclusion assay. Finally, cells were seeded directly into 3D microtissues or onto cell culture plates coated with poly-d-lysine (PDL). Cortical neurons were maintained in Neurobasal-A media with 1% penicillin/streptomycin, 0.5 mM Glutamax, and 1x B27 growth supplement with media changes every 3-4 days.

2.3.2 3D self-assembled spheroid fabrication

Scaffold-free microtissue spheres were made using agarose gels with spherical microwells. 2% molten agarose was poured onto the spheroid micromold with 400 μm diameter round pegs from Microtissues, Inc. This resulted in agarose gels with round-bottomed microwells. Agarose gels were equilibrated in cell culture media with three media changes over 48 hours. Cell solution containing the appropriate number of cells was centrifuged and re-suspended in media. The media from the agarose gels was aspirated, and 75 μL of the cell solution was seeded in the agarose gels. Cells were allowed to settle into the microwells for 45 min, and 1 mL of media was added.

2.3.3 2D determination of optimum cell number for LDH cytotoxicity assay

Serial dilutions of cortical cells in two sets of triplicate were prepared in a PDL-coated 96-well plate. Seeding densities ranged from 0 to 64,000 cells per well. Cells were cultured for 6 days. 10 μL of Lysis Buffer (Pierce) was added to one set of triplicate wells containing cells and 167 μL of media, and 10 μL of ultrapure water was added to the other set as a control. The plate was incubated for 45 min. 50 μL of media from each sample was transferred in duplicate to a new 96-well plate. 50 μL of LDH Assay Reaction Mixture (Pierce) was added to each sample well and the plate was incubated at room temperature for 30 min while protected from light. 50 μL of Stop Solution (Pierce) was added to each sample well and absorbance measurements were taken using a UV spectrometer. The absorbance values were taken at both 490 nm and 680 nm. To determine the LDH activity, the 680 nm absorbance values were subtracted from the 490 nm absorbance.

2.3.4 3D determination of optimum cell number for LDH cytotoxicity assay

Duplicate gels of cortical cell spheroids with sizes ranging from 500 cells/spheroids to 8,000 cells/spheroid were created and maintained for either 3, 6, or 14 days. 60 μL of Lysis Buffer was added to one set of duplicate gels in 1 mL of media, and 60 μL of ultrapure water was added to the other set as a control. The plate was incubated for either 45 min or overnight. 50 μL of

media from each sample was transferred in duplicate to a new 96-well plate. 50 μL of LDH Assay Reaction Mixture was added to each sample well and the plate was incubated at room temperature for 30 min while protected from light. 50 μL of Stop Solution was added to each sample well and absorbance measurements were taken using a UV spectrometer. The absorbance values were taken at both 490 nm and 680 nm. To determine the LDH activity, the 680 nm absorbance values were subtracted from the 490 nm absorbance.

2.4 Results

2.4.1 LDH release from 2D cortical cultures was within a linear range

Optimal results from the LDH release assay requires that the number of cells used gives LDH release within the linear range. The manufacture recommends that most cell types have a linear range that falls within 2,000-20,000 cells per well of a 96-well plate. Cortical cells were plated in two-dimensions in a 96-well plate in a serial dilution ranging from 8,300 to 64,000 cells/well. Cells were completely lysed to represent maximal LDH release. Control wells were instead treated with ultrapure water to represent the spontaneous release of LDH by the cortical cells. The LDH assay was applied to the treated cells according to the manufacturer's instructions and the absorbance values were plotted. The linear range of LDH release was observed within the range of cell numbers suggested by the manufacturer, of 0-20,000 cells/well. In fact, it appears as if it is possible to use the LDH assay

for denser cortical cultures approaching 35,000 cells/well. However, above cell densities of 40,000 cells/well the release is not linear, making the assay not reliable for 2D cortical cell cultures. The absorbance values varied greatly for replicates above 40,000 cells/well, as indicated by the large error bars in Figure 2.1. Spontaneous release of LDH from unlysed cells remained at low and consistent levels for the varying cell densities.

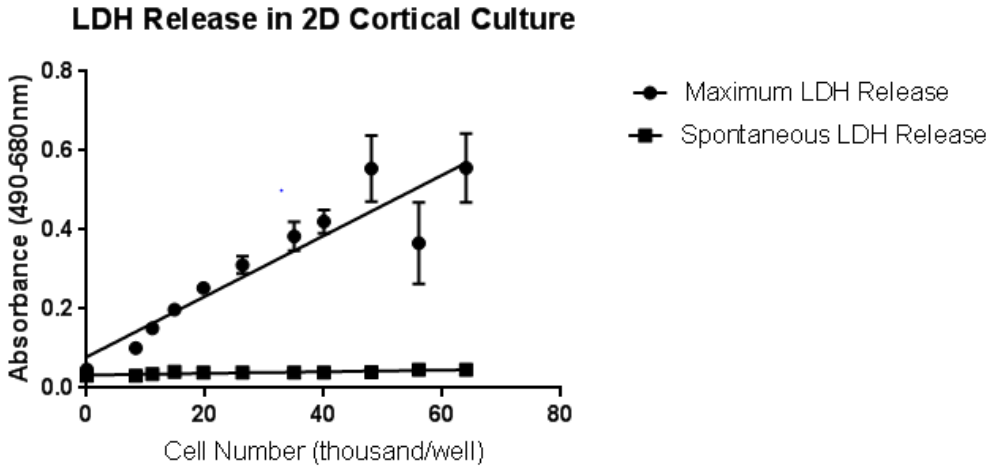

Figure 2.1 Graph of cortical cell LDH activity vs cell number

2.4.2 3D cortical cultures required a longer lysis for linear LDH release

The first attempt at using the LDH assay for 6 DIV 3D cortical spheroids was completed using the manufacturer's protocol as used for the 2D cortical cultures. Since the cortical spheroids are cultured in a 24-well plate rather than a 96-well plate, 6 times as much lysis buffer was added in order to have the same concentration of lysis buffer between the 2D and 3D cultures. The use of the manufacturer's protocol for 3D cortical spheroids resulted in

variable maximum LDH release values between replicates (Figure 2.2A). The protocol was consequently modified so that the spheroids were lysed overnight rather than for 45 min. With this modification, the absorbance values were more consistent as evident by the barely visible error bars in Figure 2.2B, and the LDH release was linear in spheroids ranging from 1,000 cells to 4,000 cells in size.

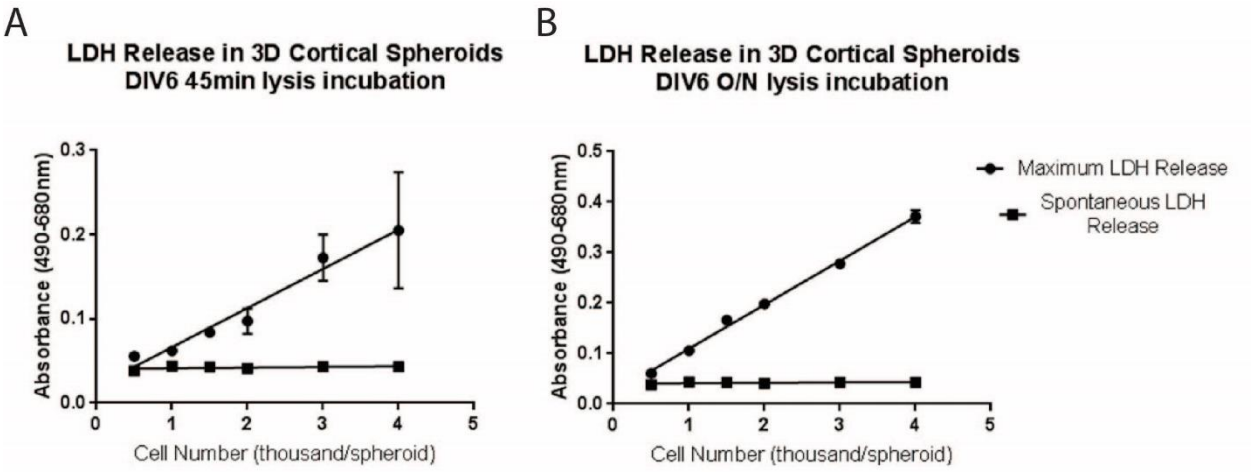

Figure 2.2 3D cortical cultures require an overnight lysis for linear LDH release. (A) Graph of LDH activity vs spheroid size with a 45 min lysis time (B) Graph of LDH activity vs spheroid size with an overnight lysis

2.4.3 The LDH assay is an effective method to determine viability in 3D cortical spheroids

Once the protocol was modified, it was essential to ensure that it was useful for a range of spheroid ages and sizes. Spheroids ranging from 1,000 to 8,000 cells in size were completely lysed overnight to represent maximal LDH release at either 3 DIV or 14 DIV. Control wells were instead treated with ultrapure water to measure the spontaneous release of LDH by the cortical

cells. The assay was applied and the absorbance readings reveal that for these conditions the LDH release in cortical spheroids is linear (Figure 2.3).

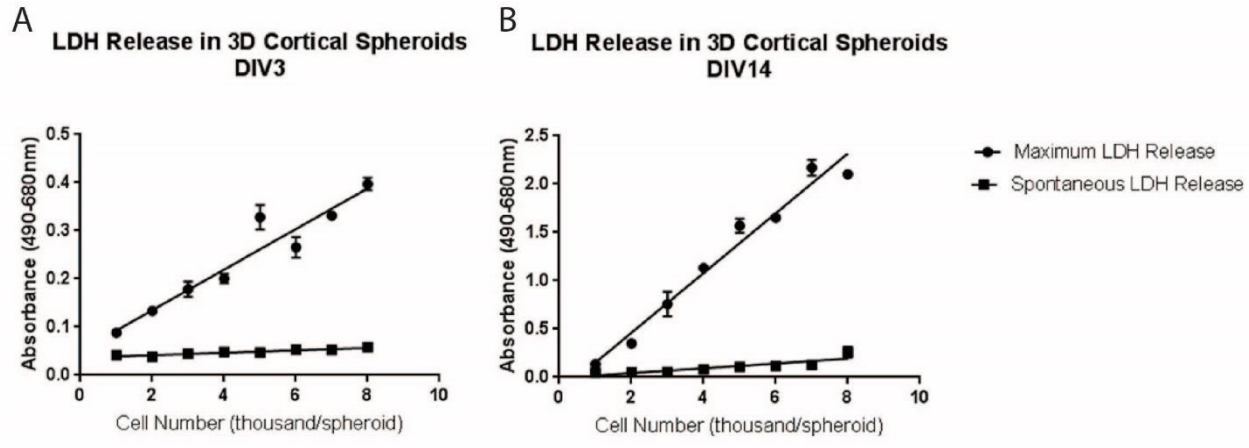

Figure 2.3 LDH release is linear in cortical spheroids within spheroid sizes of 1,000 – 8,000 cells/spheroid. This holds true for both cortical spheroids aged (A) 3 days *in vitro* and (B) 14 days *in vitro*

2.5 Discussion

Our cortical spheroid model enables the *in vitro* study of *in vivo*-relevant characteristics, such as cell density, cell composition complexity, neuronal electrophysiology, tissue stiffness, and dimensionality (Dingle, 2015). Additionally, the spheroids spontaneously self-assemble in agarose molds of 96 spheroids and on the order of thousands of spheroids can be made per neonate rat cortex, demonstrating their potential for high-throughput assays. This therefore requires the development of high-throughput screening protocols that are compatible with three-dimensional cultures. The LDH release assay is one of the most widely used methods for viability screening due to its simple and rapid procedure (Kim, 2017). The assay, which is carried out in multiwell plates, offers an advantage for testing a large number of drugs or conditions with good reproducibility. It is a challenge of

the field to find and develop assays that can handle the requirements of working in three-dimensional cultures. Therefore, the present study was carried out to develop a modified procedure of the LDH release assay to enable its application for high-throughput screening of cortical spheroid cultures.

Our first step was to validate the LDH Release Assay Kit from Pierce in order to ensure that it produced reproducible results for 2D cortical cells. We found that the kit was in fact reproducible within the linear release range between 8,300 and 35,000 cells per well as evidenced by the SEM consistently less than 0.037 between these cell densities. In order for the 3D spheroids to also have reproducible linear maximum release of LDH, the spheroids needed to be lysed for longer times. Determining the maximum release of LDH requires that all of the cells present are lysed so that the LDH present in the media is directly proportional to cell number. We therefore hypothesize that cells in the spheroids remained alive after 45 min of lysing. Spheroids required longer times to lyse completely so that the lysis buffer could diffuse throughout the entirety of the spheroids. With this small modification, the amount of LDH released from the lysed spheroids was consistent between samples, suggesting that the spheroids were completely lysed and the assay was reproducible. Additionally, we found that the ages of spheroids and range of spheroid size for which LDH release is linear fell within a range that is

experimentally useful. An interesting aspect is that the absorbance values are much higher for the older DIV14 condition than for the younger spheroids. This could potentially be due to loss of cell viability that occurs as the cells age.

Confirming that LDH release is an effective viability assay for 3D cortical spheroids gives rise to the possibility of using our spheroid model for toxicity and injury studies. The LDH release assay is simple, rapid, and can be utilized with other assays because only media aliquots are needed for the assay.

Future directions include to use the LDH release assay modified for 3D cortical spheroids as a tool to validate injury models of the CNS. It will also be essential to optimize and modify other common viability assays for three-dimensions such as the MTT assay and the Resazurin assay (Hill, 2008; Ivanov, 2013) as well as output methods with more specific applications for CNS studies such as neurotransmitter release and quantification (Simão, 2015).

2.6 References

Dingle, Y.-T. L., Boutin, M. E., Chirila, A. M., Livi, L. L., Labriola, N. R., Jakubek, L. M., … Hoffman-Kim, D. (2015). Three-Dimensional Neural Spheroid Culture: An In Vitro Model for Cortical Studies. Tissue Engineering. Part C, Methods, 21(12), 1274–83. http://doi.org/10.1089/ten.TEC.2015.0135

Hill, E. J., Woehrling, E. K., Prince, M., & Coleman, M. D. (2008). Differentiating human NT2/D1 neurospheres as a versatile in vitro 3D model system for developmental neurotoxicity testing. *Toxicology*, *249*(2–3), 243–250. http://doi.org/10.1016/j.tox.2008.05.014

Ho, W. Y., Yeap, S. K., Ho, C. L., Rahim, R. A., & Alitheen, N. B. (2012). Development of Multicellular Tumor Spheroid (MCTS) Culture from Breast Cancer Cell and a High Throughput Screening Method Using the MTT Assay. *PLoS ONE*, *7*(9), e44640. http://doi.org/10.1371/journal.pone.0044640

Ivanov, D. P., Parker, T. L., Walker, D. A., Alexander, C., Ashford, M. B., Gellert, P. R., & Garnett, M. C. (2014). Multiplexing Spheroid Volume, Resazurin and Acid Phosphatase Viability Assays for High-Throughput Screening of Tumour Spheroids and Stem Cell Neurospheres. *PLoS ONE*, *9*(8), e103817. http://doi.org/10.1371/journal.pone.0103817

Kim, Y., Kim, Y. S., Noh, M.-Y., Lee, H., Joe, B., Kim, H. Y., … Park, J. (2017). Neuroprotective effects of a novel Poly (ADP-Ribose) Polymerase-1 inhibitor, JPI-289, in hypoxic rat cortical neurons. *Clinical and Experimental Pharmacology and Physiology*. http://doi.org/10.1111/1440-1681.12757

Lee, J., Lilly, G. D., Doty, R. C., Podsiadlo, P., & Kotov, N. A. (2009). In vitro Toxicity Testing of Nanoparticles in 3D Cell Culture. *Small*, *5*(10), NA-NA. http://doi.org/10.1002/smll.200801788

Li, Q., Zhu, Y., & Jiang, H. (2008). Isoflurane preconditioning activates HIF-1α, iNOS and Erk1/2 and protects against oxygen–glucose deprivation neuronal injury. *Brain Research*, *1245*, 26–35. http://doi.org/10.1016/j.brainres.2008.09.069

Lyons, S. A., & Kettenmann, H. (1998). Oligodendrocytes and Microglia Are Selectively Vulnerable to Combined Hypoxia and Hypoglycemia Injury in Vitro. *Journal of Cerebral Blood Flow & Metabolism*, *18*(5), 521–530. http://doi.org/10.1097/00004647-199805000-00007

Ohmori, T., Hirashima, Y., Kurimoto, M., Endo, S., & Takaku, A. (1996). In vitro hypoxia of cortical and hippocampal CA1 neurons: glutamate, nitric oxide, and platelet activating factor participate in the mechanism of selective neural death in CA1 neurons. *Brain Research*, *743*(1–2), 109–15. Retrieved from http://www.ncbi.nlm.nih.gov/pubmed/9017237

Pierce LDH Cytotoxicity Assay Kit. (2014). Thermo Fisher Scientific.

Ruscher, K., Freyer, D., Karsch, M., Isaev, N., Megow, D., Sawitzki, B., … Meisel, A. (2002). Erythropoietin is a paracrine mediator of ischemic tolerance in the brain: evidence from an in vitro model. *The Journal of Neuroscience : The Official Journal of the Society for*

Neuroscience, *22*(23), 10291–301. Retrieved from http://www.ncbi.nlm.nih.gov/pubmed/12451129

Simão, D., Pinto, C., Piersanti, S., Weston, A., Peddie, C. J., Bastos, A. E. P., … Alves, P. M. (2015). Modeling Human Neural Functionality *In Vitro* : Three-Dimensional Culture for Dopaminergic Differentiation. *Tissue Engineering Part A*, *21*(3–4), 654–668. http://doi.org/10.1089/ten.tea.2014.0079

Xu, L., Sapolsky, R. M., & Giffard, R. G. (2001). Differential Sensitivity of Murine Astrocytes and Neurons from Different Brain Regions to Injury. *Experimental Neurology*, *169*(2), 416–424. http://doi.org/10.1006/exnr.2001.7678

Chapter 3: The Development of a Three Dimensional Cortical Spheroid *in vitro* Model of Ischemic Stroke

3.1 Abstract

Ischemic stroke, a major cause of morbidity and mortality worldwide, occurs when there is a localized reduction in regional blood flow in the brain resulting in an undersupply of oxygen and nutrients. We have begun to develop and characterize a three-dimensional *in vitro* model of ischemic stroke using primary cortical spheroids. The spheroids were deprived of oxygen and glucose for 24 hours using glucose-free media and anaerobic culturing conditions, and then allowed to recover in normoxic conditions to model reperfusion. The extent of injury was characterized using the LDH cell viability assay optimized to our cortical spheroids and immunohistochemistry. Age and size of the cortical spheroids impacts the resulting cell viability after ischemic injury. Additionally, ischemic injury affects various neuronal cell types present in the spheroids. Further development of this injury model provides the potential for a relevant and tailorable *in vitro* platform for ischemic injury.

3.2 Introduction

Ischemic stroke is a major cause of morbidity and mortality worldwide. According to the American Heart Association and the National Institute of

Neurological Disease and Stroke, an estimated 795,000 Americans suffer a stroke each year, with ~87% being ischemic. Stroke accounts for over 220,000 deaths annually, the fourth leading cause of death overall behind cardiac disease, cancer, and chronic lower respiratory disease. It is the leading cause of long-term disability in the US, with about one-fourth of the survivors needing assistance with daily life (Grupke, 2015).

Ischemic stroke occurs when there is a localized reduction in regional blood flow in the brain (Kalogeris, 2012). The reduction of blood flow leads to the undersupply of oxygen and nutrients, and diminished clearance of metabolic toxins, resulting in cell death (Boehm-Sturm, 2013; Grupke 2015). The brain is particularly sensitive to ischemia because it has a high metabolic demand, constituting 20-25% of total body oxygen consumption. The brain requires glucose as an energy substrate yet has low levels of stored glucose. Furthermore, the brain also has high levels of polyunsaturated fatty acids which are highly susceptible to oxidative damage (Kalogeris, 2012).

Sensitivity to ischemia varies between cell populations in the brain. Generally, neurons are the most easily damaged followed by oligodendrocytes, microglia, then astrocytes, which tend to recover (Xu, 2001). Astrocytes have glycogen stores that can have a beneficial effect on their own and on neuronal survival (Lyons, 1998). However, astrocytes also actively

participate in stroke pathology, and stimulate inflammatory genes in brain endothelial cells (Holloway, 2016).

The brain requires a continuous supply of oxygen and glucose to maintain normal function and viability. Loss of blood flow for only a few minutes can trigger a cascade of events leading to cell death such as ATP depletion, loss of metabolic function, acidosis, cytotoxic efflux of glutamate, and ionic imbalance (Goldberg, 1993; Tornabene, 2016). Reperfusion of the tissue induces subsequent damage due to a surge in the generation of reactive oxygen species (ROS) and infiltration of pro-inflammatory neutrophils (Kalogeris, 2012).

Excitotoxicity occurs during ischemia when ATP depletion leads to the failure of ion pumps that maintain membrane polarization (Grupke, 2015). Cytosolic pH drops and the cell compensates by pumping out protons in exchange for Na+ ions. Na+ ions are in turn exchanged for Ca2+ ions, which rise to cytotoxic levels (Kalogeris, 2012). Another major source of calcium overload is related to glutamate, the most abundant neurotransmitter. Glutamate, which itself has neurotoxic effects, accumulates in the extracellular space during ischemia as a consequence of energy and ion pump failure, as well as failure of reuptake mechanisms (Pellegrini-Giampietro, 1990; Moskowitz, 2010). This leads to prolonged and excessive activation of the glutamate receptor

NMDA which enhances the uptake of Ca2+ (Moskowitz, 2010; Nishizawa, 2001). As a consequence of loss of ionic homeostasis, cells swell and membranes rupture (Moskowitz, 2010). Dysfunction also occurs in the endoplasmic reticulum where proteins are misfolded or unfolded due to the ischemic stress (Kalogeris, 2012).

Reentry of oxygenated blood into ischemic tissue, while necessary for restoration of aerobic ATP production, also results in the production of ROS. Owing to their highly reactive nature, ROS generated upon reperfusion can oxidatively modify virtually every type of biomolecule found in cells, thereby inducing cell dysfunction. ROS mediate dysfunction in cell signaling pathways that are sensitive to redox changes or by modifying regulatory proteins. The primary ROS produced in ischemia/reperfusion is the superoxide anion radical (Kalogeris, 2012). Reactive nitrogen species are also mediators in ischemic injury by inhibiting key mitochondrial enzymes, facilitating mitochondrial transition pore formation, damaging DNA, and activating of Ca2+-permeable channels (Moskowitz, 2010).

Necrosis and apoptosis are the principal mechanisms of cell death after ischemic injury (Moskowitz, 2010). Necrosis is characterized by cell and organelle swelling, mitochondrial dysfunction, lack of nuclear fragmentation, plasma membrane rupture, and leakage of intracellular contents. It is

believed to occur by random, uncontrolled processes. Apoptosis occurs when stress induces the translocation of pro-death members of the Bcl2 protein family into the outer mitochondrial membrane where they permeabilize it, enabling the release of apoptotic proteins. (Kalogeris, 2012).

During ischemia, the brain develops adaptive mechanisms in an attempt to maintain normal physiological conditions (Sharp, 2004). Hypoxia-inducible factor-1 (HIF-1) is a transcription factor that has many target genes which are involved in cellular and systemic responses to ischemia including erythropoiesis, angiogenesis, vasomotor regulation, cell proliferation and survival, energy metabolism, and others (Pichiule, 2007; Sharp, 2004).

HIF-1 is a heterodimeric protein consisting of two subunits, HIF-1α and HIF-1ß. Both subunits belong to a family of basic helix-loop-helix transcription factors. HIF-1ß is a common binding partner for other members of the family, and it is constitutively expressed. HIF-1α is unique to HIF-1 and its expression is primarily regulated by oxygen tension. While the HIF-1ß gene is expressed continuously during normoxia, the HIF-1α protein is rapidly degraded (Chavez, 2002). In the presence of oxygen, HIF-1α is hydroxylated in the cytoplasm, thereby targeting it for proteasomal degradation (Sharp, 2004). In ischemia, the hydroxylases are inhibited and HIF-1α rapidly accumulates. (Sharp, 2004). HIF-1α translocates to the nucleus where it

binds to HIF-1ß and forms the active HIF-1 complex (Pichiule, 2007). HIF-1 accumulates as early as 1 hour after injury and elevated levels persist for at least 7 days (Chavez, 2002).

Some of the important HIF-1 target genes include inducible nitric oxide synthase and adrenomedullin, which produce vasodilation of cerebral blood vessels and increase blood flow, glucose transporter 1, erythropoietin, and vascular endothelial growth factor (Chavez, 2002; Sharp 2004).

Ischemia can be modeled *in vitro* by the removal of oxygen and glucose. Oxygen can be removed by either chemical or physical methods. Chemical methods involve using substances such as rotenone, antimycin, or sodium azide to inhibit the electron transport chain. Physical oxygen deprivation is caused by culturing the cells in a hypoxia chamber. Glucose is removed by culturing the cells in a glucose-free salt solution or culture media, or in the presence of 2-deoxyglucose which is an isomer of l-glucose, and cannot be metabolized (Holloway, 2016).

When compared to animal-based *in vivo* models of stroke, *in vitro* models exhibit several advantages. First, it is more straightforward to study the effect of ischemia on cell death without the complication of other cells from other organs. Second, the complex intracellular signaling pathways between

cells in culture and their potential role in the disease process can be easily investigated. Third, one can easily control the experimental condition by modulating the oxygen and glucose levels (Yang, 2012).

In the present study, our goal was to develop a 3D *in vitro* model of ischemic stroke and characterize the resulting injury. Our model was created using cortical spheroids which compounds the advantages of *in vitro* stroke models with the *in vivo*-relevance of the cortical spheroids. We determined that age and size of the cortical spheroids impacts the resulting cell viability after ischemic injury. We selected 4,000 cell spheroids cultured for 14 days *in vitro* as our 3D tissue, and found that ischemic injury affects various neuronal cell types present in the spheroids.

3.3 Methods

3.3.1 Cell culture

Primary cortical tissues were dissected from postnatal day 1-3 rats. The cell isolation protocol was modified from BrainBits. Tissues were cut into small pieces and digested in papain solution (2 mg/mL of papain in Hibernate A without calcium) for 30 min at 30°C. Papain solution was removed and replaced with a Hibernate A buffer solution (Hibernate A supplemented with 0.5 mM Glutamax and 1x B27 growth supplement). The tissues were triturated with a fire polished pasteur pipette and centrifuged at 150 xg for 5 min. The supernatant was removed, the cell pellet was re-suspended in

Neurobasal A media, and the cell solution was passed through a 40 μm cell strainer to remove debris. The cell solution was once again centrifuged at 150 xg for 5 min, re-suspended in Neurobasal A media, and strained. Cell viability was determined at the time of isolation by a trypan blue exclusion assay. Finally, cells were seeded directly into 3D microtissues or onto cell culture plates coated with poly-d-lysine. Cortical neurons were maintained in Neurobasal-A media with 1% penicillin/streptomycin, 0.5 mM Glutamax, and 1x B27 growth supplement with media changes every 3-4 days.

3.3.2 3D self-assembled spheroid fabrication

Scaffold-free microtissue spheres were made using agarose gels with spherical microwells. 2% molten agarose was poured onto the spheroid micromold with 400 μm diameter round pegs from Microtissues, Inc. This resulted in agarose gels with round-bottomed microwells. Agarose gels were equilibrated in cell culture media with three media changes over 48 hours. Cell solution containing the appropriate number of cells was centrifuged and re-suspended in media. The media from the agarose gels was aspirated, and 75 μL of the cell solution was seeded in the agarose gels. Cells were allowed to settle into the microwells for 45 min, and 1 mL of media was added.

3.3.3 Oxygen glucose deprivation

4,000 and 8,000 cell cortical spheroids were exposed to oxygen glucose deprivation (OGD) with glucose free media and the GasPak EZ Anaerobe Container System. Media used for OGD consisted of Glucose-Free and

Sodium Pyruvate-Free Neurobasal-A media with 1% penicillin/streptomycin and 1×Antioxidant-Free B27 growth supplement. GasPak is an incubation system designed for culturing anaerobic bacteria. Cells are placed into the airtight container along with a sachet containing inorganic carbonate, activated carbon, ascorbic acid, and water that is activated upon opening to lower the oxygen concentration to less than 1% within 2.5 hours. Spheroids were removed from complete cortical media, placed in OGD media, and incubated in the GasPak Container for 24 hr at 37°C. Spheroids were then either immediately fixed or allowed to recover in complete cortical media. Recovery time was either 24 hours, 3 days, or 7 days.

3.3.4 Lactate dehydrogenase (LDH) cytotoxicity assay

A LDH cytotoxicity kit (Pierce) was used to quantify cell cytotoxicity based on membrane permeability. Permeabilized cells release a stable cytoplasmic enzyme, LDH, as an indicator of being damaged or lysed. 50 µL media aliquots were taken from spheroid samples that were exposed to either normoxic or ischemic conditions. The amount of LDH in the media was quantified using the cytotoxicity kit. In brief, 50 µL of LDH Assay Reaction Mixture was added to each sample well and the plate was incubated at room temperature for 30 min while protected from light. 50 µL of Stop Solution was added to each sample well and absorbance measurements were taken using a UV spectrometer. The absorbance values were taken at both 490 nm and 680 nm. To determine the LDH activity, the 680 nm absorbance values

were subtracted from the 490 nm absorbance. The absorbance values of media blanks were taken as well and subtracted from the experimental measurements. Absorbance values were normalized by using a fold change calculation in which the OGD absorbance values were divided by the mean of the normoxia absorbance values.

3.3.5 Whole spheroid immunostaining and optical clearing

Spheroids were fixed in 4% v/v paraformaldehyde and 8% w/v sucrose in PBS overnight, followed by three 30 min PBS washes. All of the following steps were performed on a shaker at room temperature. Spheroids were permeabilized and blocked with 10% normal goat serum, 4% bovine serum albumin, and 1% Triton X-100 in PBS for 2 hours, and subsequently incubated in primary antibody diluted in blocking solution overnight. The following day, the spheroids underwent two 2 hour washes in 0.2% Triton X-100 in PBS followed by 2 hour blocking in blocking solution. Spheroids were incubated in secondary antibody diluted in blocking solution overnight. The following day, the spheroids underwent three 30 min washes in 0.2% Triton X-100 in PBS and incubated in 1ug/mL of 4',6-diamidino-2-phenylindole (DAPI) in PBT for 1 hr and returned to PBS.

Antibody	Dilution	Company Catalog #
Primary Antibodies		
Mouse monoclonal anti-ß-III-tubulin	1:50	Biolegend 801202
Mouse monoclonal anti-O1	1:50	Millipore MAB344
Secondary Antibodies		
Cy3 goat anti-mouse	1:500	Jackson 111-165-068

The ClearT2 solutions and protocol was used for optical clearing. Briefly, spheres were incubated in: 1) 25% formamide/10% poly-ethylene glycol (PEG) for 10 min, 2) 50% formamide/20% PEG for 5 min, and 3) 50% formamide/20% PEG for 60 min. Spheroids were kept in final clearing solution and transferred to glass-bottom confocal dishes for imaging on a Zeiss LSM 510 Meta Confocal Laser Scanning Microscope.

3.4 Results

3.4.1 Lactate dehydrogenase activity in response to injury depends on the age and size of cortical spheroids

4,000 cell and 8,000 cell primary rat cortical spheroids were exposed to 24 hours of oxygen/glucose deprivation at either 3, 7 or 14 days *in vitro*. The viability of the cortical spheroids was assessed using the LDH cytotoxicity assay either immediately after injury or after a recovery period in normoxic conditions of 24 hours, 3 days, or 7 days. LDH activity of the injured spheroids was normalized to control spheroids of the same age that remained in normoxic conditions.

Injured 3 DIV cortical spheroids had very little LDH activity for both 4,000 and 8,000 cell spheroids. For the 4,000 cell spheroids, the difference in raw absorbance values between the OGD condition and its paired control were not statistically significant except for the 7 day recovery condition where the

normoxic control had more LDH activity than the injured spheroids (Figure 3.1). There was a statistically significant difference between the injured and control 8,000 spheroids for all but one recovery time (3 days). However, the fold change of absorbance remained low compared to other experimental conditions (Figure 3.2A & B).

7 DIV spheroids exposed to OGD had different LDH activity depending on their size. Similarly to the 3 DIV spheroids, injured 7 DIV 8,000 cell spheroids had low levels of LDH activity comparable to the control samples as evidenced by the small fold changes (Figure 3.2D). 7 DIV 4,000 cell spheroids had much greater fold changes than the larger spheroid size (Figure 3.2C). The extent of the LDH activity dropped in the injured spheroids with longer recovery until by 7 days of recovery, the raw absorbance values of the OGD and normoxia samples were no longer significantly different (Supplementary Figure 3.1).

Injured 14 DIV cortical spheroids had much greater LDH activity than the normoxia controls as seen by the high fold changes. The extent of the LDH activity dropped with more recovery time. Spheroids given 24 hours of recovery in normoxic conditions had the greatest LDH activity that was significantly different than the LDH activity immediately following injury (4k $p= 0.0009$, 8k $p< 0.0001$) (Figure 3.2E & F). The condition that resulted in the

largest fold change of LDH activity was 4,000 cell 14 DIV spheroids with either no recovery or 24 hour recovery. For this reason this size and age of spheroid and recovery conditions were selected for use in the following experiments.

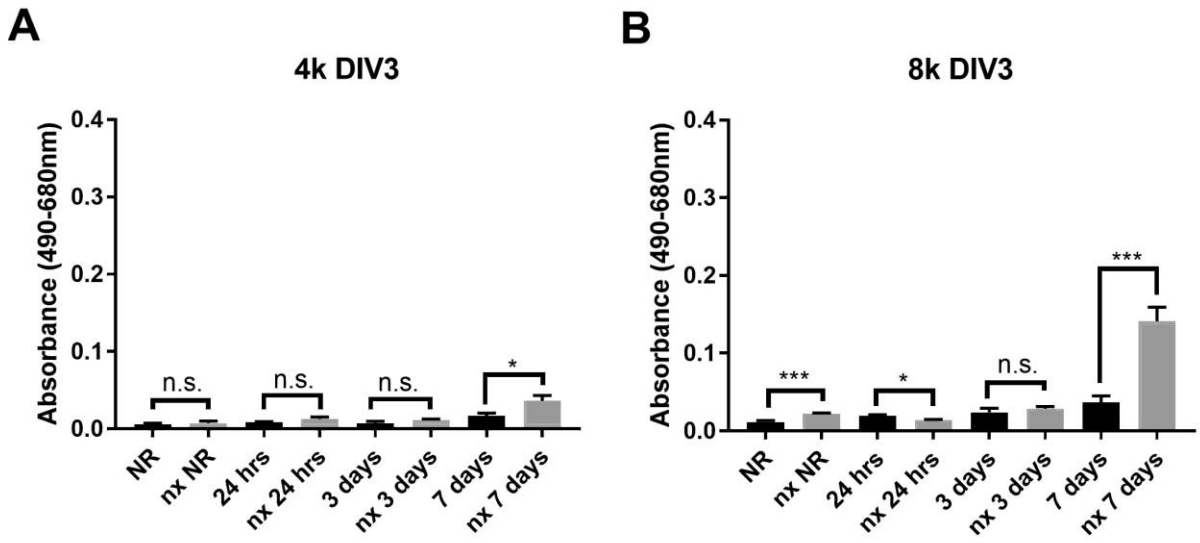

Figure 3.1 LDH cytotoxicity assay absorbance values for 4k (A) and 8k (B) cortical spheroids cultured for 3 days *in vitro* prior to injury. Samples with no, 24 hour, 3 day, or 7 day recovery are compared to their normoxia control using unpaired t-tests *p: 0.01-0.05, **p: 0.001-0.01, ***p: 0.0001-0.001, ****p<0.001.

3.4.2 Neuronal cell types are influenced by exposure to oxygen/glucose deprivation

4,000 cell cortical spheroids were exposed to OGD at 14 DIV and either fixed immediately or allowed to recover for 24 hours in normoxic conditions prior to fixation. Following fixation, the spheroids were stained with either ß-III-tubulin or O1 to visualize neurons and oligodendrocytes, respectively.

ß-III-tubulin staining reveals that OGD injury disrupted neuronal networks in the spheroids. The staining pattern in injured spheroids is more punctate without clear connections between cells. There are also regions of bright staining surrounding DAPI-positive nuclei (Figure 3.3).

Preliminary images of the oligodendrocytes do not present as clear of a difference in the staining between conditions. It is possible that there are more brightly stained cell bodies in the injured cortical spheroids (Figure 3.4). However, more evaluation is required to further evaluate this claim.

Figure 3.2 Fold changes of LDH cytotoxicity assay absorbance data calculated by dividing OGD absorbance values by the average normoxia control absorbance value. Horizontal line represents mean. No recovery and 24 hr recovery fold changes compared for 14 DIV samples using unpaired t-tests ***p: 0.0001-0.001, ****p<0.001.

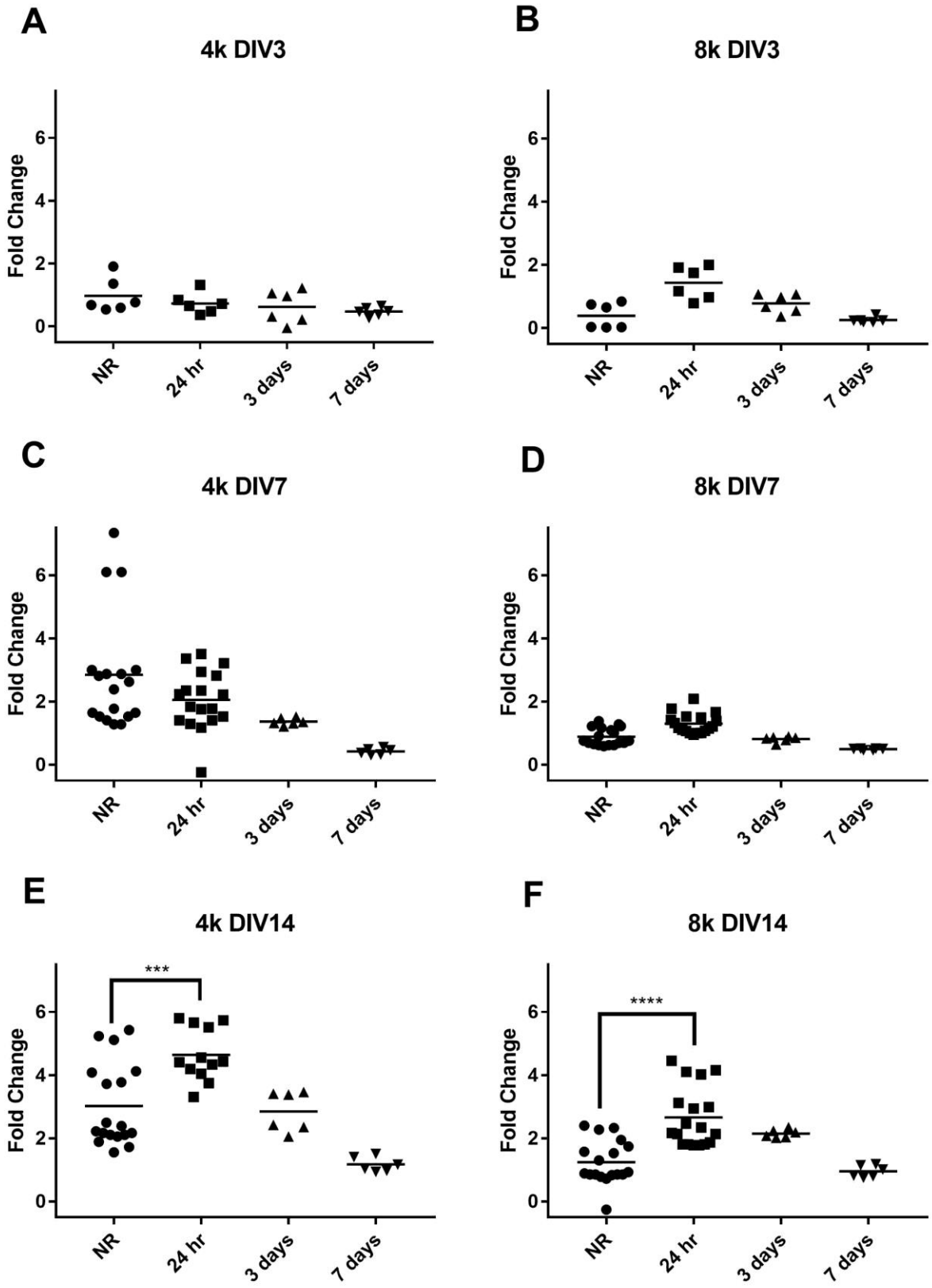
A
4k DIV3
B
8k DIV3
C
4k DIV7
D
8k DIV7
E
4k DIV14
F
8k DIV14
Fold Change
0
2
4
6
NR
24 hr
3 days
7 days
***
****

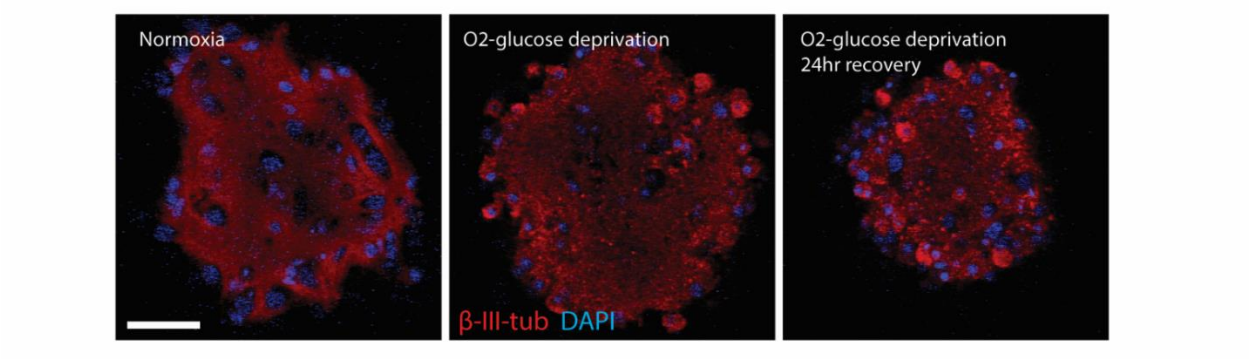

Figure 3.3 Confocal z-slice projection of 4,000 cell 14 DIV spheroids stained for ß-III-tubulin (red) and DAPI (blue). Scale bar, 50 µm

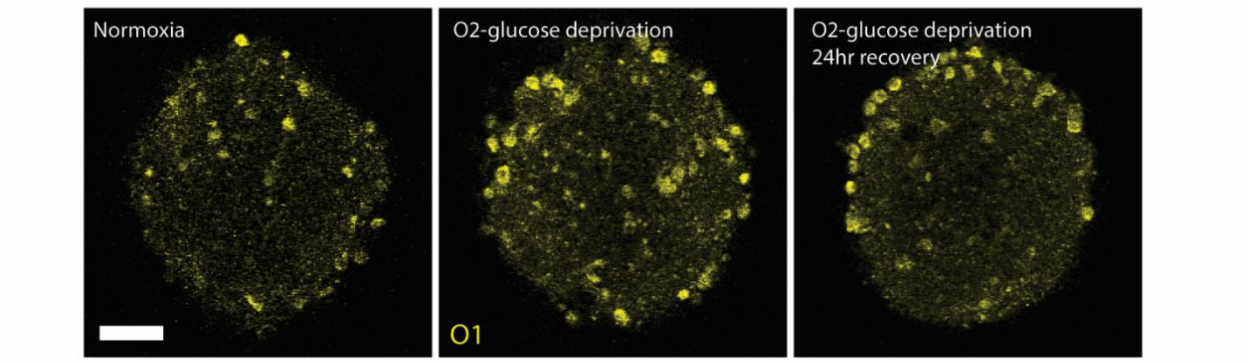

Figure 3.4 Confocal z-slice projection of 4,000 cell 14 DIV spheroids stained for O1 (yellow). Scale bar, 50 µm

3.5 Discussion

We have begun to develop and characterize a three-dimensional *in vitro* model of ischemic stroke using primary cortical spheroids. Oxygen/glucose deprivation is caused by using glucose-free media and an anaerobic environment created and maintained by the GasPak EZ Anaerobe Container System. An ideal characterization of an ischemic injury model would display the impact of the injury on overall cell viability, the selective vulnerability of the various neural cell types present in the model, and the presence of signaling molecules known to be influential in the response to injury. In this

study we developed a mechanism of injury and determined the proper age and size of the spheroid for the model. Additionally, we began to characterize the injury in multiple cell types.

The LDH cytotoxicity assay, which has been confirmed to be an effective viability assay for 3D cortical spheroids, allowed us to distinguish differences in response to OGD between spheroid sizes and ages. 3 DIV spheroids had very little cell death after injury while 14 DIV spheroids were much more sensitive to the injury condition. Many *in vitro* models of ischemic stroke use cells that have been cultured for at least 14 days so that they express relevant neurotransmitter receptors (Freese, 1992; von Engelhardt, 2007; Weaver, 1997). It is therefore likely that our primary cortical spheroids did not express the proper neurotransmitter receptors prior to 14 DIV resulting in little to no cytotoxic response to injury. For this reason 14 DIV spheroids were selected for our injury model.

8,000 cell spheroids consistently had smaller LDH fold changes than 4,000 cell spheroids of the same age and recovery conditions. This suggests that the 8,000 cell injured spheroids had similar cell viability to the 8,000 cell control spheroids. However it is interesting to note that the 8,000 cell normoxia spheroids had much higher baseline LDH activity (Supplementary Figure 3.2) than the 4,000 cell normoxia spheroids. The reason the larger spheroids

have a lower cell viability could be due to a necrotic core. Regardless of the reason, the lower cell viability in the control makes the fold change values low and difficult to determine how much of the cytotoxic response is due to the injury. Therefore, the smaller 4,000 cell spheroids were selected for the injury model.

For all of the ages and sizes of spheroids, the extent of LDH activity dropped with more recovery time. This is expected to be a result of multiple media changes that occurred during the recovery period. Therefore, the LDH activity taken at a recovery time point does not represent the overall cell death since injury but rather represents the cell death that occurred between media changes within the recovery phase. However, the comparison between no recovery and 24 hour recovery conditions is significant. All recovered cells had a media change to restore them to normoxia making the LDH activity representative of the cell death that occurred during this 24 hour recovery. The fold change for 24 hour recovery was larger than the fold change for no recovery in a significant manner for 14 DIV spheroids. The observation that the recovery period was more cytotoxic to the spheroids than the injury itself is supported by the experiments in which reperfusion of the tissue with oxygenated blood produces reactive oxygen species and results in a secondary injury (Kalogeris, 2012). For this reason, no recovery and 24 hour recovery

were selected as the most relevant conditions to be included in the injury model.

Our selected ischemic injury model uses 14 DIV 4,000 cell primary cortical spheroids that are exposed to OGD for 24 hours. Subsequently, the spheroids are immediately analyzed or allowed to recover in normoxic conditions for an additional 24 hours. Future experiments can be performed to modify the model by varying the length of the injury. *In vitro* stroke models do not have a standard length of injury and the duration of OGD can vary between studies from 5 minutes to 2 days (Günther, 2004; Ohmori, 1996).

With our established injury model, we began to characterize the effect of OGD on various cortical cell types. This was performed through immunostaining for ß-III-tubulin and O1 to visualize neurons and oligodendrocytes, respectively. There was a clear visual difference in the staining for neurons, suggesting that the neuronal networks and cell health are impacted by the ischemic injury. It was less clear whether the oligodendrocytes were impacted using the O1 stain. Future experiments will include a more in depth analysis of the O1 staining patterns with a larger sample size of injured cortical spheroids. Previous studies have shown that ischemia and reperfusion cause fragmentation and arborization of oligodendrocyte processes (Lyons, 1998; McIver, 2010). Oligodendrocyte

processes were not visible in our spheroids using the O1 stain and therefore future experiments will include using an alternative stain selective for oligodendrocytes that clearly labels both proximal and distal processes. We also plan to characterize the effect of ischemia on other neural cell types including microglia, astrocytes, and neural progenitor cells.

When developing a 3D *in vitro* ischemic injury model, it is crucial that we characterize the injury on a molecular level. *In vivo* ischemia induces a multitude of molecular responses including ion imbalance, the activation of cell death pathways, and adaptive responses. Future studies will need to address these molecular phenomena in order to claim that our 3D *in vitro* ischemia model has *in vivo* relevance. Analyses will be run on extracellular calcium and potassium concentrations (Schiff, 1987). Western blots will be performed for proteins involved in cell death pathways. Example targets include MMP-2, MMP-9, PARP1, and bcl-2 family proteins (Gu, 2005; Hill, 2012; Li, 2008; Xu, 2001). The amount of transcription factor HIF-1-α, which is involved in response to injury, will be quantified using both Western blots and RT-qPCR (Li, 2008).

3.6 References

Boehm-Sturm, P., Farr, T. D., Adamczak, J., Jikeli, J. F., Mengler, L., Wiedermann, D., … Hoehn, M. (2013). Vascular changes after stroke in the rat: a longitudinal study using optimized magnetic resonance imaging. *Contrast Media & Molecular Imaging*, *8*(5), 383–392. http://doi.org/10.1002/cmmi.1534

Chavez, J. C., & LaManna, J. C. (2002). Activation of hypoxia-inducible factor-1 in the rat cerebral cortex after transient global ischemia: potential role of insulin-like growth factor-1. *The Journal of Neuroscience : The Official Journal of the Society for Neuroscience*, *22*(20), 8922–31. Retrieved from http://www.ncbi.nlm.nih.gov/pubmed/12388599

Freese, A., Finklestein, S. P., & DiFiglia, M. (1992). *Basic fibroblast growth factor protects striatal neurons in vitro from NMDA-receptor mediated excitotoxicity*. *Brain Research* (Vol. 575). Retrieved from http://www.sciencedirect.com/science/article/pii/000689939290104H

Goldberg, M. P., & Choi, D. W. (1993). Combined oxygen and glucose deprivation in cortical cell culture: calcium-dependent and calcium-independent mechanisms of neuronal injury. *The Journal of Neuroscience : The Official Journal of the Society for Neuroscience*, *13*(8), 3510–24. Retrieved from http://www.ncbi.nlm.nih.gov/pubmed/8101871

Grupke, S., Hall, J., Dobbs, M., Bix, G. J., & Fraser, J. F. (2015). Understanding history, and not repeating it. Neuroprotection for acute ischemic stroke: From review to preview. *Clinical Neurology and Neurosurgery*, *129*, 1–9. http://doi.org/10.1016/j.clineuro.2014.11.013

Gu, Z., Cui, J., Brown, S., Fridman, R., Mobashery, S., Strongin, A. Y., & Lipton, S. A. (2005). A Highly Specific Inhibitor of Matrix Metalloproteinase-9 Rescues Laminin from Proteolysis and Neurons from Apoptosis in Transient Focal Cerebral Ischemia. *Journal of Neuroscience*, *25*(27), 6401–6408. http://doi.org/10.1523/JNEUROSCI.1563-05.2005

Günther, A., Manaenko, A., Franke, H., Wagner, A., Schneider, D., Berrouschot, J., & Reinhardt, R. (2004). Hyperbaric and normobaric reoxygenation of hypoxic rat brain slices – impact on purine nucleotides and cell viability. *Neurochemistry International*, *45*(8), 1125–1132. http://doi.org/10.1016/j.neuint.2004.06.013

Hill, J. W., Poddar, R., Thompson, J. F., Rosenberg, G. A., & Yang, Y. (2012). Intranuclear matrix metalloproteinases promote DNA damage and apoptosis induced by oxygen–glucose deprivation in neurons. *Neuroscience*, *220*, 277–290. http://doi.org/10.1016/j.neuroscience.2012.06.019

Holloway, P. M., & Gavins, F. N. E. (2016). Modeling Ischemic Stroke In Vitro: Status Quo and Future Perspectives. *Stroke*, *47*(2), 561–569. http://doi.org/10.1161/STROKEAHA.115.011932

Kalogeris, T., Baines, C. P., Krenz, M., & Korthuis, R. J. (2012). Cell Biology of Ischemia/Reperfusion Injury. In *International review of cell and molecular biology* (Vol. 298, pp. 229–317). http://doi.org/10.1016/B978-0-12-394309-5.00006-7

Li, Q., Zhu, Y., & Jiang, H. (2008). Isoflurane preconditioning activates HIF-1α, iNOS and Erk1/2 and protects against oxygen–glucose deprivation neuronal injury. *Brain Research*, *1245*, 26–35. http://doi.org/10.1016/j.brainres.2008.09.069

Lyons, S. A., & Kettenmann, H. (1998). Oligodendrocytes and Microglia Are Selectively Vulnerable to Combined Hypoxia and Hypoglycemia Injury in Vitro. *Journal of*

Cerebral Blood Flow & Metabolism, *18*(5), 521–530. http://doi.org/10.1097/00004647-199805000-00007

McIver, S. R., Muccigrosso, M., Gonzales, E. R., Lee, J. M., Roberts, M. S., Sands, M. S., & Goldberg, M. P. (2010). Oligodendrocyte degeneration and recovery after focal cerebral ischemia. *Neuroscience*, *169*(3), 1364–75. http://doi.org/10.1016/j.neuroscience.2010.04.070

Moskowitz, M. A., Lo, E. H., & Iadecola, C. (2010). The Science of Stroke: Mechanisms in Search of Treatments. *Neuron*, *67*(2), 181–198. http://doi.org/10.1016/j.neuron.2010.07.002

Nishizawa, Y. (2001). Glutamate release and neuronal damage in ischemia. *Life Sciences*, *69*(4), 369–81. Retrieved from http://www.ncbi.nlm.nih.gov/pubmed/11459428

Ohmori, T., Hirashima, Y., Kurimoto, M., Endo, S., & Takaku, A. (1996). In vitro hypoxia of cortical and hippocampal CA1 neurons: glutamate, nitric oxide, and platelet activating factor participate in the mechanism of selective neural death in CA1 neurons. *Brain Research*, *743*(1–2), 109–15. Retrieved from http://www.ncbi.nlm.nih.gov/pubmed/9017237

Pellegrini-Giampietro, D. E., Cherici, G., Alesiani, M., Carla, V., & Moroni, F. (1990). Excitatory amino acid release and free radical formation may cooperate in the genesis of ischemia-induced neuronal damage. *The Journal of Neuroscience : The Official Journal of the Society for Neuroscience*, *10*(3), 1035–41. Retrieved from http://www.ncbi.nlm.nih.gov/pubmed/1969465

Pichiule, P., Chavez, J. C., Schmidt, A. M., & Vannucci, S. J. (2007). Hypoxia-inducible Factor-1 Mediates Neuronal Expression of the Receptor for Advanced Glycation End Products following Hypoxia/Ischemia. *Journal of Biological Chemistry*, *282*(50), 36330–36340. http://doi.org/10.1074/jbc.M706407200

Schiff, S. J., & Somjen, G. G. (n.d.). The effect of graded hypoxia on the hippocampal slice: an in vitro model of the ischemic penumbra. *Stroke*, *18*(1), 30–7. Retrieved from http://www.ncbi.nlm.nih.gov/pubmed/3027927

Sharp, F. R., & Bernaudin, M. (2004). HIF1 and oxygen sensing in the brain. *Nature Reviews Neuroscience*, *5*(6), 437–448. http://doi.org/10.1038/nrn1408

Tornabene, E., & Brodin, B. (2016). Stroke and Drug Delivery— In Vitro Models of the Ischemic Blood-Brain Barrier. *Journal of Pharmaceutical Sciences*, *105*(2), 398–405. http://doi.org/10.1016/j.xphs.2015.11.041

von Engelhardt, J., Coserea, I., Pawlak, V., Fuchs, E. C., Köhr, G., Seeburg, P. H., & Monyer, H. (2007). Excitotoxicity in vitro by NR2A- and NR2B-containing NMDA receptors. *Neuropharmacology*, *53*(1), 10–17. http://doi.org/10.1016/j.neuropharm.2007.04.015

Weaver, C. E., Park-Chung, M., Gibbs, T. T., & Farb, D. H. (1997). *17β-Estradiol protects against NMDA-induced excitotoxicity by direct inhibition of NMDA receptors*. *Brain Research* (Vol. 761). Retrieved from http://www.sciencedirect.com/science/article/pii/S0006899397004496

Xu, L., Sapolsky, R. M., & Giffard, R. G. (2001). Differential Sensitivity of Murine Astrocytes and Neurons from Different Brain Regions to Injury. *Experimental Neurology*, *169*(2), 416–424. http://doi.org/10.1006/exnr.2001.7678

Yang, L., Shah, K. K., & Abbruscato, T. J. (2012). An In Vitro Model of Ischemic Stroke. In *Methods in molecular biology (Clifton, N.J.)* (Vol. 814, pp. 451–466). http://doi.org/10.1007/978-1-61779-452-0_30

3.7 Supplementary Materials

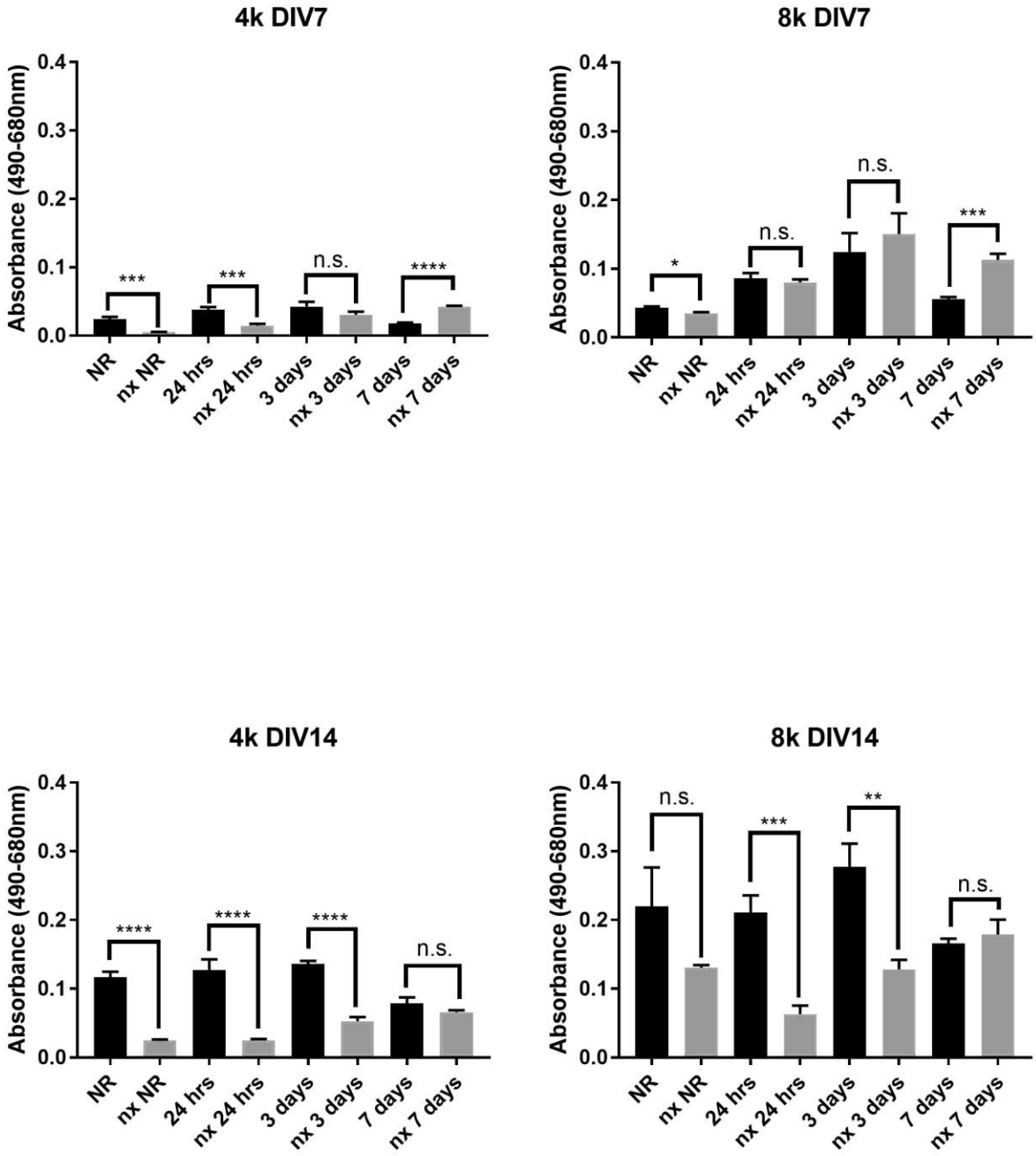

Supplementary Figure 3.1 LDH cytotoxicity assay absorbance values for 4k and 8k cortical spheroids cultured for 7 or 14 days *in vitro* prior to injury. Samples with no, 24 hour, 3 day, or 7 day recovery are compared to their normoxia control using unpaired t-tests *p: 0.01-0.05, **p: 0.001-0.01, ***p: 0.0001-0.001, ****p<0.001.

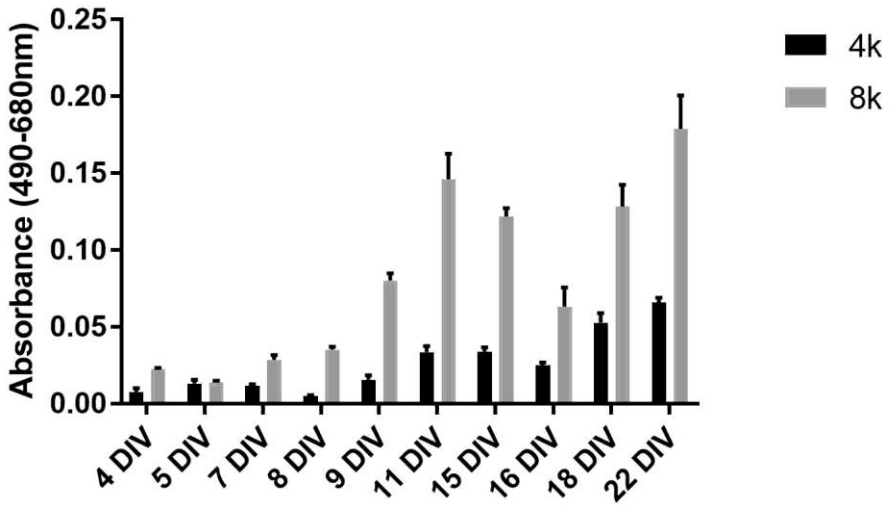

Supplementary Figure 3.2 LDH cytotoxicity assay absorbance values for normoxia 4k and 8k cortical spheroids of a variety of ages. Spheroids have more LDH activity with increased size and age.

Chapter 4: The Dynamics of Capillary-Like Networks in Three-Dimensional Cortical Spheroids After Ischemic Injury

4.1 Abstract

The pathology of ischemic stroke includes dysfunction of the blood brain barrier. First, the barrier breaks down and becomes more permeable. In the second phase of events, there is vascular remodeling and angiogenesis. Within our three-dimensional cortical spheroids, cortical endothelial cells spontaneously assemble into capillary-like network structures. This allows for the study of the neurovasuculature during ischemic injury. The spheroids were deprived of oxygen and glucose for 24 hours using glucose-free media and anaerobic culturing conditions, and then allowed to recover in normoxic conditions to model reperfusion. The impact of ischemia on the capillary-like networks was determined using immunohistochemistry for laminin, a well-established biomarker for neural vasculature. The networks are dynamic and responded to ischemic injury by losing their tubular structures and forming rings in the center of the spheroids. Future works aim to further understand the dynamics of capillary-like network response to ischemic injury and the cells involved.

4.2 Introduction

Neurovascular dysfunction is linked to many CNS diseases – such as stroke, traumatic brain injury, and Alzheimer's Disease – which makes the understanding of the neurovasculature and its dysfunction essential for the development of therapeutics. A CNS disease of interest that disrupts the neurovasculature is ischemic stroke, for which our lab is developing a 3D *in vitro* model.

Following ischemic stroke there is a cascade of biochemical events that lead to disruption and remodeling of the blood brain barrier (BBB) in two phases: the acute and chronic phases. During the acute phase, the BBB breaks down and becomes more permeable. In the chronic phase, there is remodeling of the BBB and angiogenesis (Vallon, 2014). Oxidative damage and the presence of free radicals contributes to BBB dysfunction immediately following stroke through several mechanisms (Obermeier, 2013). Oxidative stress disrupts tight junction proteins which increases the permeability of the barrier (Prakash, 2015). Pro-inflammatory cytokines and matrix metalloproteinases are upregulated and activated, both of which remodel and break down the extracellular matrix (Vallon, 2014). Astrocytes also contribute actively to the breakdown of the BBB. Astrocytic end feet detach from the endothelium, which contributes to the disassembly of tight junction complexes. In addition, astrocytes release a wide range of chemical mediators such as chemokines,

pro-inflammatory and anti-inflammatory cytokines, and growth factors which trigger BBB opening and changes in transporter expression (Tornabene, 2016).

In the chronic phase, there is the formation of new vessels by angiogenesis, an important process that is hypothesized to participate in brain plasticity and functional recovery after stroke (Liu, 2014). Angiogenesis is a process in which endothelial cells proliferate and vessels sprout to eventually increase vascular density (Prakash, 2015). This is a highly regulated and step-wise process with important steps including degradation of surrounding matrix, proliferation and migration of endothelial cells, recruitment of pericytes, and stabilization and cessation of newly formed vessels (Vallon, 2014). This requires an orchestrated interplay of many stimulators, inhibitors and matrix components including VEGF. Ischemia induces VEGF expression in a variety of cell types including macrophages, pericytes, vascular smooth muscles cells and astrocytes (Ogunshola, 2000). In animal models of stroke, the proliferation of endothelial cells appears as early as 12–24 h after ischemia and persists for up to several weeks thereafter (Liu, 2014; Prakash, 2015). Increased vascular density is observed within 3 days after stroke (Prakash, 2015).

The presence of capillary-like networks (CLNs) in our primary rat cortical spheroids allows for the study of the neurovasculature under pathological conditions including ischemic stroke. In the present study, our goal was to characterize the behavior of self-assembling capillary-like networks in cortical spheroids that were exposed to oxygen/glucose deprivation. The networks are dynamic and respond to ischemic injury.

4.3 Methods

4.3.1 Cell culture

Primary cortical tissues were dissected from postnatal day 1-3 rats. The cell isolation protocol was modified from BrainBits. Tissues were cut into small pieces and digested in papain solution (2 mg/mL of papain in Hibernate A without calcium) for 30 min at 30°C. Papain solution was removed and replaced with a Hibernate A buffer solution (Hibernate A supplemented with 0.5 mM Glutamax and 1x B27 growth supplement). The tissues were triturated with a fire polished pasteur pipette and centrifuged at 150 xg for 5 min. The supernatant was removed, the cell pellet was re-suspended in Neurobasal A media, and the cell solution was passed through a 40 µm cell strainer to remove debris. The cell solution was once again centrifuged at 150 xg for 5 min, re-suspended in Neurobasal A media, and strained. Cell viability was determined at the time of isolation by a trypan blue exclusion assay. Finally, cells were seeded directly into 3D microtissues or onto cell culture plates coated with poly-d-lysine. Cortical neurons were maintained in

Neurobasal-A media with 1% penicillin/streptomycin, 0.5 mM Glutamax, and 1x B27 growth supplement with media changes every 3-4 days.

4.3.2 3D self-assembled spheroid fabrication

Scaffold-free microtissue spheres were made using agarose gels with spherical microwells. 2% molten agarose was poured onto the spheroid micromold with 400 μm diameter round pegs from Microtissues, Inc. This resulted in agarose gels with round-bottomed microwells. Agarose gels were equilibrated in cell culture media with three media changes over 48 hours. Cell solution containing the appropriate number of cells was centrifuged and re-suspended in media. The media from the agarose gels was aspirated, and 75 μL of the cell solution was seeded in the agarose gels. Cells were allowed to settle into the microwells for 45 min, and 1 mL of media was added.

4.3.3 Oxygen glucose deprivation

4,000 or 8,000 cell 3DIV cortical spheroids were exposed to oxygen glucose deprivation (OGD) with glucose free media and the GasPak EZ Anaerobe Container System. Media used for OGD consisted of Glucose-Free and Sodium Pyruvate-Free Neurobasal-A media with 1% penicillin/streptomycin and 1×Antioxidant-Free B27 growth supplement. GasPak is an incubation system designed for culturing anaerobic bacteria. Cells are placed into the airtight container along with a sachet containing inorganic carbonate, activated carbon, ascorbic acid, and water that is activated upon opening to lower the oxygen concentration to less than 1% within 2.5 hours. Spheroids

were removed from complete cortical media, placed in OGD media, and incubated in the GasPak Container for 24 hr at 37°C. Spheroids were then either immediately fixed or allowed to recover for 24 hours in complete cortical media.

4.3.4 Whole spheroid immunostaining and optical clearing

Spheroids were fixed in 4% v/v paraformaldehyde and 8% w/v sucrose in PBS overnight, followed by three 30 min PBS washes. All of the following steps were performed on a shaker at room temperature. Spheroids were permeabilized and blocked with 10% normal goat serum, 4% bovine serum albumin, and 1% Triton X-100 in PBS for 2 hours, and subsequently incubated in primary antibody diluted in blocking solution overnight. The following day, the spheroids underwent two 2 hour washes in 0.2% Triton X-100 in PBS followed by 2 hour blocking in blocking solution. Spheroids were incubated in secondary antibody diluted in blocking solution overnight. The following day, the spheroids underwent three 30 min washes in 0.2% Triton X-100 in PBS and incubated in 1ug/mL of 4',6-diamidino-2-phenylindole (DAPI) in PBT for 1 hour and returned to PBS.

Antibody	Dilution	Company Catalog #
Primary Antibody		
Rabbit polyclonal anti-laminin	1:100	BTI BT-594
Secondary Antibody		
Cy3 goat anti-rabbit	1:200	Jackson 111-165-144

The ClearT2 solutions and protocol were used for optical clearing. Briefly, spheres were incubated in: 1) 25% formamide/10% poly-ethylene glycol (PEG) for 10 min, 2) 50% formamide/20% PEG for 5 min, and 3) 50% formamide/20% PEG for 60 min. Spheroids were kept in final clearing solution and transferred to glass-bottom confocal dishes for imaging on a Zeiss LSM 510 Meta Confocal Laser Scanning Microscope.

4.4 Results

Immunohistochemistry for laminin (Ln), a well-established biomarker for neural vasculature, was performed to visualize the capillary-like networks formed by endothelial cells. Normoxia control spheroids at 3 DIV had extended Ln-positive tubular structures, as previously characterized by our lab. The majority of spheroids exposed to OGD at 3 DIV both with and without recovery had previously unseen laminin features. Spheroids had a concentric ring of bright Ln staining in the center of the spheroid (Figure 4.1). Spheroids that did not contain either CLNs or rings were either featureless or contained dense Ln-positive nodules as characterized previously. To estimate the frequency with which these Ln features appeared, approximately 25 spheroids per experimental condition were examined. The percent of spheroids in normoxia that had CLNs was 78% for 8,000 cell spheroids and 73% for 4,000 cell spheroids. Spheroids exposed to OGD without recovery exhibited much fewer CLNs with 7% for 8k and 12% for 4k. Meanwhile, the injured spheroids contained many ring structures

with 81% for 8k and 52% for 4k. The majority of spheroids that were recovered for 24 hours also exhibited rings with 47% for 8k and 62% for 4k (Figure 4.2).

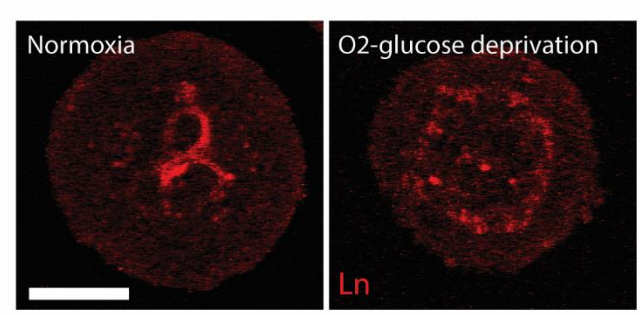

Figure 4.1 Confocal z-slice projection of spheroids stained for Ln (red). Scale bar 100 µm

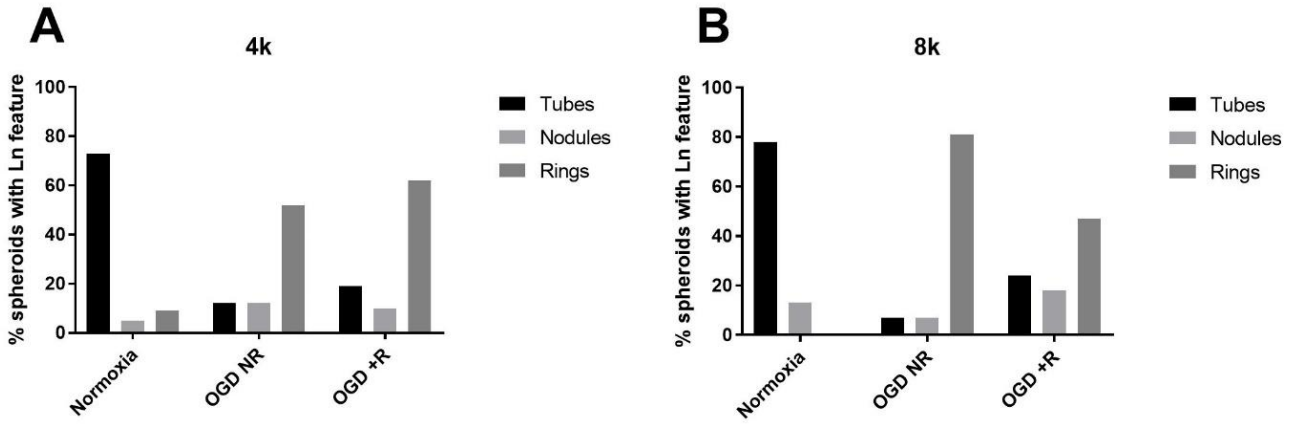

Figure 4.2 Graphs of percent of 4,000 cell (A) or 8,000 cell (B) spheroids with laminin structures.

4.5 Discussion

As our lab begins to develop and characterize our 3D *in vitro* model of ischemia, it is important to characterize the impact of injury on various cell types, structures, and signaling molecules present in the model. Since neurovascular dysfunction is linked to the pathology of ischemic stroke, it is

essential to investigate the influence of our engineered injury on the capillary-like networks present in the cortical spheroids.

In the present study, primary cortical spheroids aged three days *in vitro* were exposed to 24 hours of oxygen/glucose deprivation. It is at this age that the CLNs are the most frequent and extensive. Following injury and reperfusion, very few CLN structures were present. Instead they were replaced by concentric rings of bright laminin staining. This suggests that the CLNs are dynamic structures that respond to ischemic injury. Counting the number of spheroids with distinct Ln features was performed only once and with a small sample size of approximately 25 spheroids per condition. We therefore aim to perform this experiment several more times in the future.

Future directions also include experiments to further understand the dynamics of CLN response to injury and the cells involved. This will include immunostaining for CD31 to label endothelial cells and the use of spheroids with endogenously labeled ECs. Endogenously labeled ECs will allow for real-time imaging of the network dynamics after injury and during the reperfusion phase.

Previous studies have shown that ischemic injury causes the disassembly of tight junction complexes during the acute phase (Prakash, 2015; Tornabene,

2016). It will therefore be interesting to investigate the tight junctions present in the spheroids possibly using a stain for zona-occuldens.

4.6 References

Liu, J., Wang, Y., Akamatsu, Y., Lee, C. C., Stetler, R. A., Lawton, M. T., & Yang, G.-Y. (2014). Vascular remodeling after ischemic stroke: Mechanisms and therapeutic potentials. *Progress in Neurobiology*, *115*, 138–156. http://doi.org/10.1016/j.pneurobio.2013.11.004

Obermeier, B., Daneman, R., & Ransohoff, R. M. (2013). Development, maintenance and disruption of the blood-brain barrier. *Nature Medicine*, *19*(12), 1584–1596. http://doi.org/10.1038/nm.3407

Ogunshola, O. O., Stewart, W. B., Mihalcik, V., Solli, T., Madri, J. A., & Ment, L. R. (2000). Neuronal VEGF expression correlates with angiogenesis in postnatal developing rat brain. *Brain Research. Developmental Brain Research*, *119*(1), 139–53. Retrieved from http://www.ncbi.nlm.nih.gov/pubmed/10648880

Prakash, R., & Carmichael, S. T. (2015). Blood–brain barrier breakdown and neovascularization processes after stroke and traumatic brain injury. *Current Opinion in Neurology*, *28*(6), 556–564. http://doi.org/10.1097/WCO.0000000000000248

Tornabene, E., & Brodin, B. (2016). Stroke and Drug Delivery— In Vitro Models of the Ischemic Blood-Brain Barrier. *Journal of Pharmaceutical Sciences*, *105*(2), 398–405. http://doi.org/10.1016/j.xphs.2015.11.041

Vallon, M., Chang, J., Zhang, H., & Kuo, C. J. (2014). Developmental and pathological angiogenesis in the central nervous system. *Cellular and Molecular Life Sciences*, *71*(18), 3489–3506. http://doi.org/10.1007/s00018-014-1625-0

Appendix: CellRox Reagent Pilot Project

A.1 Abstract

As described in Chapter 3 of this thesis, we are developing and characterizing a three-dimensional *in vitro* model of ischemic stroke using postnatal rat primary cortical spheroids. There are cascades of events that lead to cell death and tissue damage both during loss of blood flow and reperfusion. Reactive oxygen species (ROS) are formed during reperfusion and induce cellular dysfunction (Goldberg, 1993; Kalogeris, 2012). The following pilot experiment was performed to determine if there was an increase in ROS present in injured cortical spheroids. This was performed using CellRox Green or CellRox Deep Red Reagents – cell-permeable dyes exhibit bright fluorescence upon oxidation by ROS. With the current protocol, it is unclear whether there is a difference in fluorescence for the different experimental conditions. Further development of this or other ROS assays are required to fully understand the formation of ROS in injured cortical spheroids.

A.2 Methods

The presence of reactive oxygen species in primary cortical spheroids was determined using CellRox Green or CellRox Deep Red Reagents. These cell-permeable dyes exhibit bright fluorescence upon oxidation by ROS. CellRox dye stock solutions of 2.5mM in DMSO were diluted in cell media to a final concentration of 5uM. Spheroids were incubated in CellRox for 1.5 hours at

37°C. The media was then removed, spheroids were washed 3 times in PBS and then fixed in 4% v/v paraformaldehyde and 8% w/v sucrose in PBS for 1.5 hours, followed by three 10 min PBS washes. Spheroids were then removed from the agarose gels and optically cleared using the ClearT2 protocol described previously, and transferred to glass-bottom confocal dishes for imaging.

A.3 Results

Normoxia spheroids dyed with Cellrox Green had pixelated staining that looked very similar to the type of signal found in background staining. However, the pixels were denser and the outline of the spheroid was distinguishable from the background (Figure A.1A). OGD spheroids without recovery looked very similar to the normoxia control (Figure A.1B). The Cellrox Deep Red stain did not label the normoxia spheroids. They were indistinguishable from the background (Figure A.1C). The OGD spheroids without recovery looked similar to those stained with Cellrox Green with a highly pixelated stain making outlining the shape of the spheroid (Figure A.1D).

Due to the poor fluorescent labeling of the OGD and normoxia no recovery spheroids, we experimented with the confocal microscope settings on the second day of imaging for the 24 hour recovery spheroids. The microscope setting that greatly impacted the confocal images was the size of the pinhole.

Cellrox Green imaged with the pinhole at the optimal size of one airy disk (65 μm) resulted in staining that was faint for both normoxia and OGD (Figure A.2A & B). When imaged with a larger pinhole of 896 μm, the images were much less pixelated and the cells were distinguishable. The normoxia spheroids had a darker stain in the core (Figure A.2C). The OGD spheroids had similar-looking cores. However the OGD spheroids also had small bright cells in the early sections (Figure A.2D).

The Cellrox Deep Red stain imaged with the pinhole at the optimal size of one airy disk (82 μm) resulted in pixelated staining with darker cells scattered throughout the spheroid. Both conditions had this appearance (Figure A.3A & B). A larger pinhole of 896 μm made the stain appear cloudy and the OGD samples may be slightly darker (Figure A.3C & D).

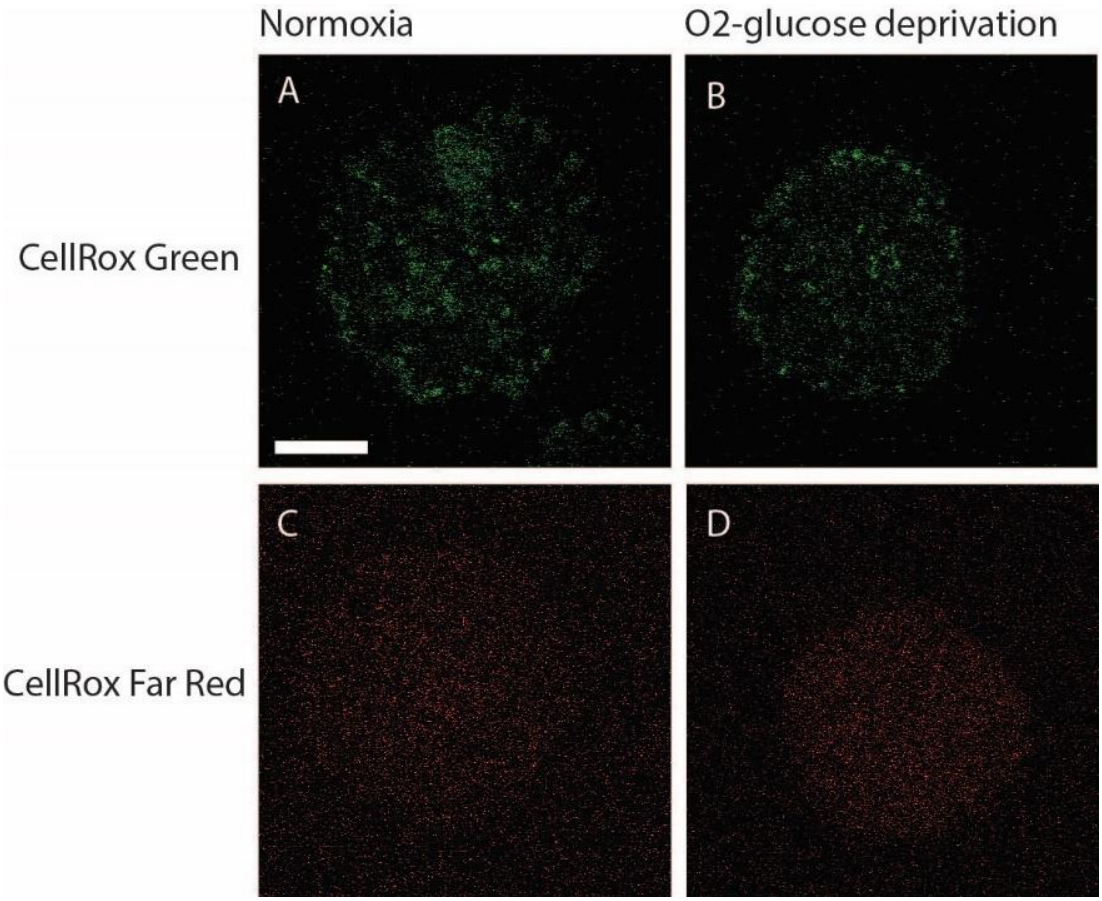

Figure A.1 Confocal z-slice projection of 4,000 cell 14 DIV spheroids stained with CellRox Green (green) or CellRox Far Red (red). Scale bar, 100 μm

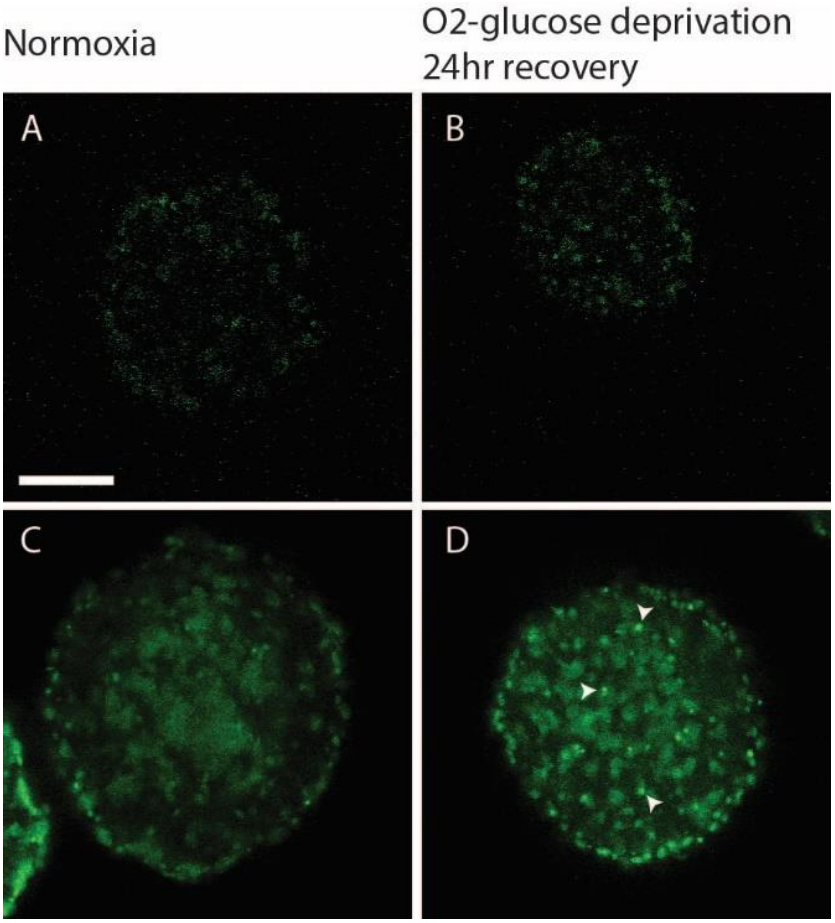

Figure A.2 Confocal z-slice projection of 4,000 cell 14 DIV spheroids stained with CellRox Green (green). Images were taken with a pinhole size of 65 μm (A, B) or 896 μm (C, D). White arrowheads highlight small, bright, CellRox-positive cells. Scale bar, 100 μm

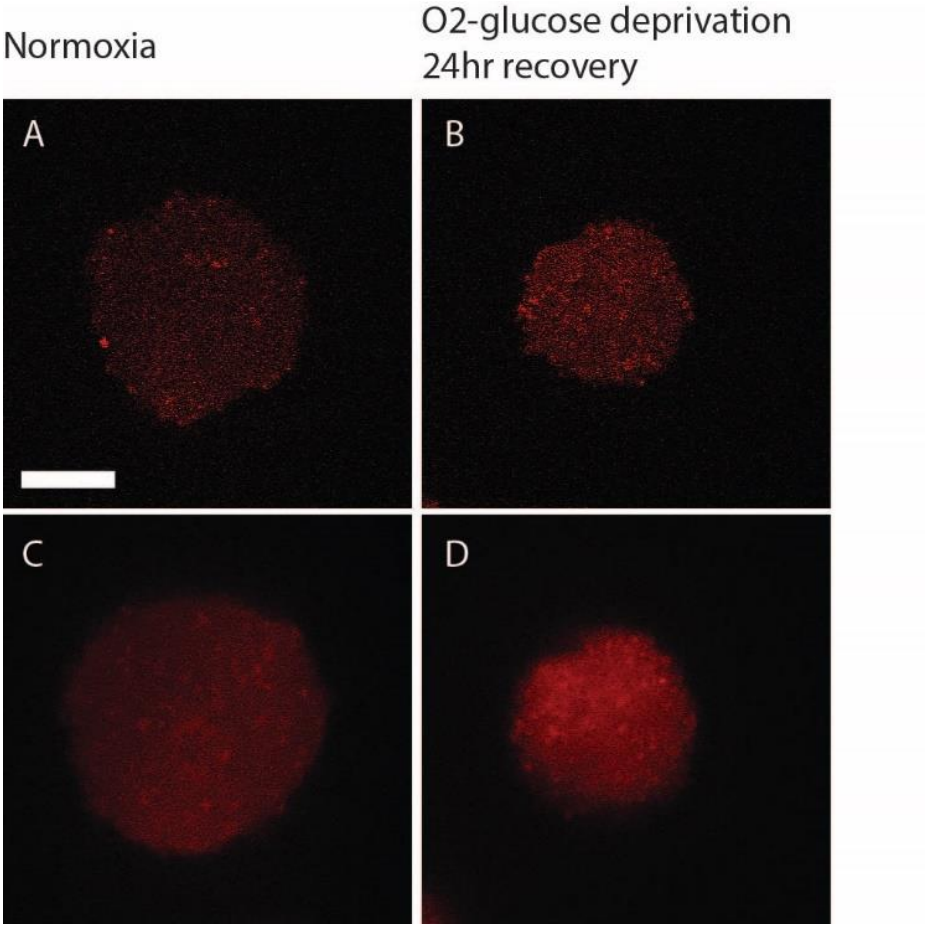

Figure A.3 Confocal z-slice projection of 4,000 cell 14 DIV spheroids stained with CellRox Far Red (red). Images were taken with a pinhole size of 82 μm (A, B) or 896 μm (C, D). Scale bar, 100 μm

A.4 Discussion

Part of the ischemic injury pathology is the production of reactive oxygen species during the reperfusion phase. ROS cause further injury by modifying virtually every type of biomolecule found in cells, and thereby inducing cell dysfunction (Kalogeris, 2012). The CellRox dyes are cell-permeable dyes that exhibit bright fluorescence upon oxidation by ROS. We therefore aimed to use the intensity of the fluorescent signal as an indicator of ROS presence in our 3D *in vitro* model of ischemic injury. However, the fluorescent signal was

very poor and the stains were not visually distinguishable between experimental conditions. Increasing the size of the pinhole made the images brighter and allowed us to better distinguish cells within the spheroids. This was expected because increasing the pinhole size allows more light to reach the detector, making the image brighter. However, this additional light is out of focus light, making the images increasingly blurry (Peters, 2016). Ideally we should optimize the CellRox staining protocol or use a different fluorescent dye so that we can image using the optimized settings with a pinhole size of one airy disk.

A.5 References

Goldberg, M. P., & Choi, D. W. (1993). Combined oxygen and glucose deprivation in cortical cell culture: calcium-dependent and calcium-independent mechanisms of neuronal injury. *The Journal of Neuroscience : The Official Journal of the Society for Neuroscience*, *13*(8), 3510–24. Retrieved from http://www.ncbi.nlm.nih.gov/pubmed/8101871

Kalogeris, T., Baines, C. P., Krenz, M., & Korthuis, R. J. (2012). Cell Biology of Ischemia/Reperfusion Injury. In *International review of cell and molecular biology* (Vol. 298, pp. 229–317). http://doi.org/10.1016/B978-0-12-394309-5.00006-7

Peters, N. (2016). W. M. Keck Microscopy Center. Retrieved from http://depts.washington.edu/keck/leica/pinhole.htm